Journal of Sedimentary Research

Journal of Sedimentary Research, 2013, v. 83, 0–0
Research Article
DOI: 10.2110/jsr.2013.22

DISTINGUISHING SIMILAR VOLCANIC SOURCE AREAS FROM AN INTEGRATED PROVENANCE ANALYSIS: IMPLICATIONS FOR FORELAND ANDEAN BASINS

AUGUSTO N. VARELA,[1,2] LUCÍA E. GÓMEZ-PERAL,[1,2] SEBASTIÁN RICHIANO,[1,2] AND DANIEL G. POIRÉ[1,2]
[1]*Centro de Investigaciones Geológicas, (CONICET–UNLP), Calle 1 644, 1900 La Plata, Argentina*
[2]*Cátedras de Sedimentología y Rocas Sedimentarias, Facultad de Ciencias Naturales y Museo, Universidad Nacional de La Plata, Calle 122 y 60 s/n, La Plata, Argentina*
e-mail: augustovarela@cig.museo.unlp.edu.ar

ABSTRACT: **The Mata Amarilla Formation marks the onset of the foreland stage of the Austral basin, which is composed of mostly nonmarine and littoral siliciclastic sediments, thus providing an opportunity to study the detrital record of the Late Cretaceous southern foreland Andes. Our dataset provides, for the first time, a comprehensive picture of the Late Cretaceous evolution of the Austral foreland basin, constituting a possible analogue to other foreland basins at the foot of the Andes. Sandstones from the Mata Amarilla Formation testify to variable contributions from Jurassic bimodal volcanic rocks of the Deseado Massif and the Patagonian fold-and-thrust belt, in the context of an eastward-advancing orogen. Sandstone petrography shows an overall feldspathic litharenite composition, whereas sandstones coming from the northeast (Deseado Massif) have higher Lv and lower Qp proportions than samples coming from the west (Patagonian fold-and-thrust belt). In the central part of the study area, sandstones are characterized by higher proportions of Qt associated with a greater distance and time of transport relating to its position in the Austral foreland basin. In spite of the increased maturity of sandstone in the central area, X-ray analyses permit recognition of the compositional signature of Mata Amarilla Formation, in which four clay-mineral assemblages were identified: S (rich in smectite), S-K (rich in smectite and kaolinite), Pg (rich in palygorskite), and I/S (rich in illite–smectite mixed layers). S-assemblage evidences well-crystallized smectite, characteristic of volcaniclastic origin. Most smectite was formed during early diagenesis through alteration of labile tuffaceous material derived from the Southern Andes. The stratigraphic variations in clay-mineral assemblages reveal a strong environmental control on their distribution. The transformation of smectite into illite and kaolinite is considered as product of pedogenesis, whereas the presence of palygorskite indicates a coastal environment with paleosol development under poorly drained conditions.**

INTRODUCTION

Compositional studies are often useful for analyzing the evolution of sedimentary basins, revealing temporal and spatial variations in the participation of different sediment source areas (Dickinson and Rich 1972; Ingersoll 1983; Critelli and Ingersoll 1995; Net et al. 2002; Cavazza and Ingersoll 2005). Detrital compositions of terrigenous sediments provide a record of the tectonic setting of their provenance areas (Dickinson et al. 1983). Therefore, compositional variations constitute an important database of regional and paleogeographic changes in the source areas, which are commonly related to tectonic and magmatic activity (Zattin et al. 2003; Stefani et al. 2007; Spalletti et al. 2008; Umazano et al. 2008; Umazano et al. 2009; Hulka and Heubeck 2010). Petrographic analysis of clastic successions combined with paleocurrent data from foreland basins constitute a well-established methodology for evaluating the paleogeographic location and composition of the eroded source-rock types (Zattin et al. 2003; Stefani et al. 2007; Hulka and Heubeck 2010).

In turn, the composition of whole-rock and clay fraction obtained by X-ray diffraction depends not only on the areas of supply but also on other factors, including depositional environments and mechanisms of transport, climate, and diagenesis (Inglès and Anadón1991; Net et al. 2002; Gómez-Peral et al. 2011).

Clay-mineral assemblages that were affected only by eodiagenetic processes thereby become significant in unraveling the depositional history of fine-grained sedimentary rocks in ancient sequences. Consequently, the clay-mineral assemblages have been a useful tool to the study of a variety of sedimentary basins around the world (Chamley 1989; Inglès and Anadón 1991; Inglès and Ramos-Guerrero 1995; Adatte et al. 2002; Net 2002; Do Campo et al. 2010). Clay minerals are the common products of weathering and authigenesis, while clay assemblages are the result of the complex interaction of several variables affecting continental sediments (Do Campo et al. 2010), including source-area lithology, continental basin morphology, depositional environments, and paleoclimate (Chamley 1989).

Previous studies of diagenetic clay minerals in other units of the Austral Basin are rare (Iñiguez Rodríguez and Decastelli 1984), and detailed sandstone-provenance analyses are restricted to the Campanian–Maastrichtian and Paleocene successions (Manassero 1988; Macellari et al. 1989). Furthermore, there have been no previous compositional studies in the Mata Amarilla Formation (Fig. 1).

The Mata Amarilla Formation is 100 to 350 m thick and includes gray and black mudstones, alternating with beds of white and gray-yellow fine- and medium-grained sandstones deposited in littoral and continental environments (Russo and Flores 1972; Russo et al. 1980; Arbe 1989, 2002; Poiré et al. 2004; Varela and Poiré 2008). The succession is divided into three sections (lower, middle, and upper) on the basis of sedimentary facies analysis (Varela 2009, 2011); sedimentary facies and architectural

Published Online: Month Year
 1527-1404/13/xxx-xxx/$03.00

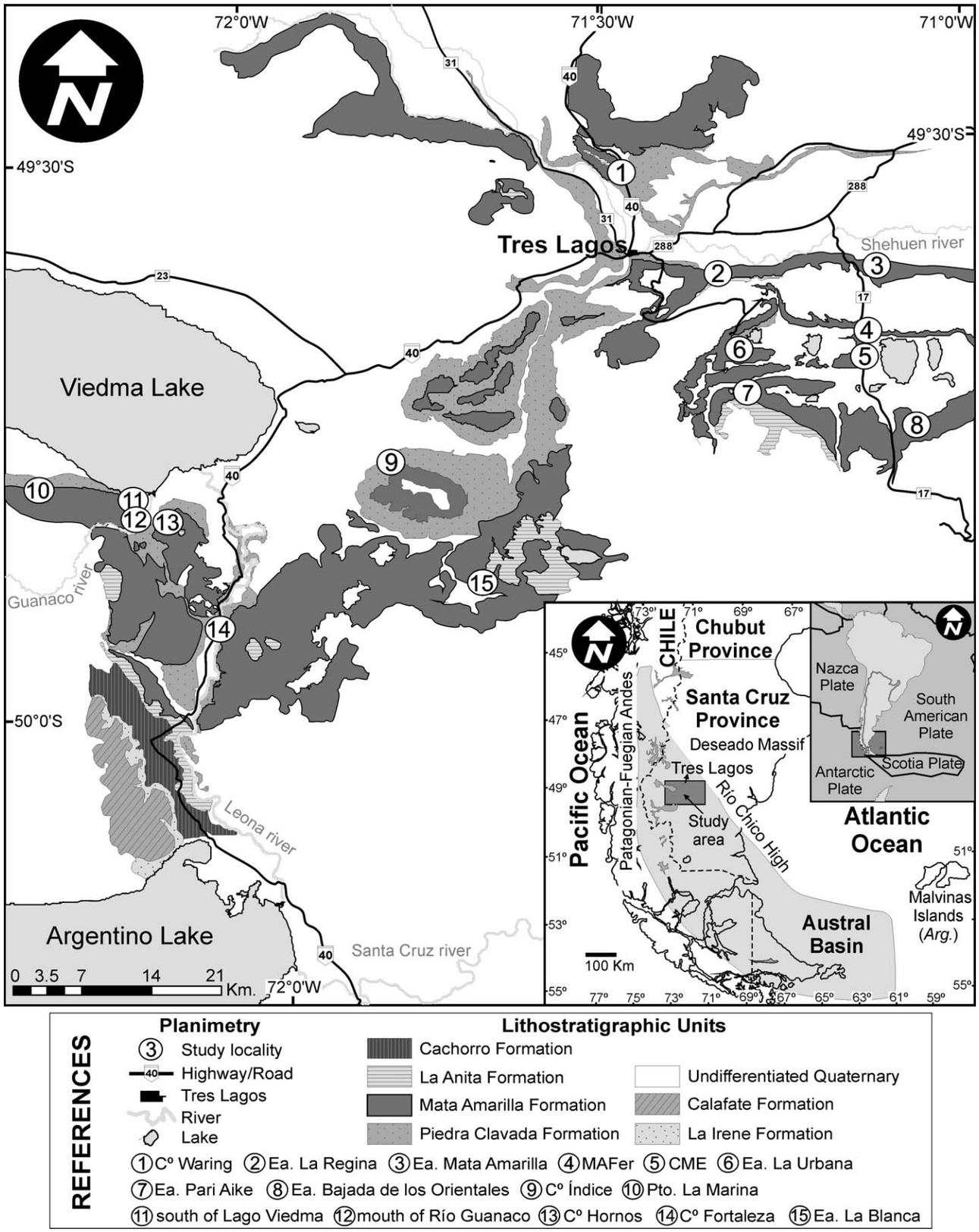

FIG. 1.—Geological setting of the Austral Basin and geological map of the study area showing the Cretaceous units (after Varela 2011).

elements demonstrate different conditions of accommodation space with respect to sediment supply and related to paleoenvironmental changes (Varela 2009, 2011).

The aim of this contribution is to provide preliminary data on the composition and provenance of the Mata Amarilla Formation, deposited in the greenhouse climate context of the Late Cretaceous. In order to complete the compositional characterization of the unit, recognized eodiagenetic processes were considered.

The Austral foreland basin exemplifies a particular case study, as the source areas, craton, orogen, and arc, consist mostly of volcanic rocks. This work illustrates how relatively minor changes in detrital modes must be considered in the context of the paleodrainage pattern, in order to recognize source areas with different ages and tectonic–geographic setting. Provenance and paleocurrent data of the Mata Amarilla Formation could be compared to other foreland basins at the foot of the Andes with similar composition and unsolved hydrographic problems.

GEOLOGICAL SETTING

History of the Austral Basin

The Austral Basin (also known towards the south as the Rocas Verdes Marginal Basin + Magallanes Basin) is located on the southwestern edge of the South American Plate, and it is bounded to the south by the Scotia Plate (Fig. 1). It extends over the southernmost end of Argentina and Chile, and is surrounded to the east by the Deseado Massif (Macizo del Deseado) and to the west by the Patagonian–Fuegian Andes (Andes Patagónico–Fueguinos, Fig. 1).

Three main tectonic stages of the Austral Basin have been identified in the study area (Biddle et al. 1986; Rodríguez and Miller 2005; Varela et al. 2012a); a rift stage, a stage of thermal subsidence, and, finally, a foreland stage.

Rift Stage.—This rifting stage is part of the Chon Aike province, which is connected with the breakup of Gondwana (Pankhurst et al. 2000). This unit is one of the largest silicic igneous provinces known, and it is composed of rhyolitic ignimbrites, which form a bimodal association with minor mafic and intermediate lavas (Pankhurst et al. 2000). Diachronism is recognized between the Early–Middle Jurassic volcanism of the Deseado Massif in eastern Patagonia (Marifil and Chon Aike formations) and the Middle Jurassic–earliest Cretaceous volcanism of the Andean Cordillera (El Quemado, Ibañez, and Tobífera formations) (Pankhurst et al. 2000). In this initial stage, grabens and half-grabens were developed and filled with volcaniclastic and volcanic rocks intercalated with some epiclastic sediments (Biddle et al. 1986).

Thermal Subsidence Stage.—Subsequent, thermal subsidence deposited the typical transgressive quartzose sandstones of the Springhill Formation. The Springhill Formation broadly overlaps the margins of the initial half-graben, and is overlain by a thick deep-marine succession, characterized by alternating black mudstones and marls of the Río Mayer Formation, which extends to the Albian (Richiano 2012). Towards the end of this stage (early Aptian–Albian), a large passive-margin delta system, the Piedra Clavada Formation, developed in the northern and eastern sectors of the basin.

Foreland Stage.—A regional change from extensional to shortening deformation took place in the Late Cretaceous; compression continued to the Neogene (Biddle et al. 1986; Wilson 1991; Spalletti and Franzese 2007; Fosdick et al. 2011). Shortening associated with the early stages of the orogeny resulted in a retroarc fold-and-thrust belt along the Patagonian–Fuegian Andes (Biddle et al. 1986; Fildani et al. 2003; Fildani and Hessler 2005; Fosdick et al. 2011; Varela et al. 2012a). This fold-and-thrust belt is associated along its eastern margin with a foreland basin (Austral Foreland Basin and Magallanes Basin). The onset of the shortening phase in the northern sector of the Austral Basin took at place about 100 Ma and is recorded by the west-to-east progradation of the fluvial–estuarine facies of the Mata Amarilla Formation (Varela 2011; Varela et al. 2012a).

Mata Amarilla Formation

This fluvial and littoral succession has been referred as "Estratos de Mata Amarilla" (Mata Amarilla Strata; Feruglio *in* Fossa Mancini et al. 1938), later formally recognized as the Mata Amarilla Formation (Leanza 1972; Russo and Flores 1972), and is synonymous with the succession that Ameghino (1906) called "Sehuenense" [*sic*] (Varela et al. 2008; Varela 2009; O'Gorman and Varela 2010). It is one of the best examples of the lower Upper Cretaceous deposits in the Austral Basin, possibly demarking the closure of the Rocas Verdes Basin (Biddle et al. 1986; Varela 2009, 2011; Varela et al. 2012a).

The Mata Amarilla Formation has a maximum thickness of approximately 350 m in outcrops, and is composed of gray and blackish siltstones and claystones alternating with beds measuring between 1 and 10 m consisting in white and yellow-grey fine- to medium-grained sandstones, deposited in littoral and continental environments (Arbe 1989; Arbe 2002; Poiré et al. 2004; Russo and Flores 1972; Russo et al. 1980; Varela and Poiré 2008; Varela 2009, 2011; Varela et al. 2011). The type locality is defined on the southern margin of the Río Shehuen or Chalía (Shehuen or Chalía River), approximately 23 km east of the locality of Tres Lagos at the Estancia Mata Amarilla (Mata Amarilla Farm, locality 3, Fig. 1). It overlies the Piedra Clavada Formation with transitional contact and is unconformably overlain by the La Anita Formation (Varela and Poiré 2008; Varela 2009, 2011) (Fig. 2). The formation (see Fig. 2) was deposited during the early Late Cretaceous, extending from the Cenomanian to the Santonian (Poiré et al. 2007; Varela and Poiré 2008; Varela 2011; Varela et al. 2012a). Recent dating, based on twenty U-Pb spot analyses by laser ablation on the outer parts of zoned zircon crystals from a tuff in the middle section of the Mata Amarilla Formation, yield a concordia age of 96.2 ± 0.7 Ma, corresponding to the middle Cenomanian (Varela et al. 2012a).

On the basis of facies analysis, Varela (2011) recently divided the Mata Amarilla Formation into three sections, according to facies analysis, which respond to different conditions of accommodation space–sediment supply (Fig. 2). The lower section of the Mata Amarilla Formation consists of mudstones and fine-grained sandstones with paleosol development, interbedded with shell beds. In the eastern part of the study area, eight littoral facies associations were recognized: coarse-grained bars, large-scale bars, bioclastic lobes, sand bars with herringbone cross-stratification, sand bars with hummocky cross-stratification, small-scale gravelly channels and diamictites, mudstones with shells pavements, and heterolithic beds with marine fossils. These facies associations are interpreted as littoral marine, lagoon, estuary, and bayhead delta paleoenvironments (Varela 2011; Varela et al. 2011). In the western sector of the basin, facies associations identified were large-scale simple ribbons and fine-grained beds, consistent with a distal fluvial system (Varela 2011; Varela et al. 2011). The paleogeography of the lower section of the Mata Amarilla Formation is interpreted as a great embayment (Varela 2011; Varela et al. 2011).

The middle section of the Mata Amarilla Formation is characterized by conglomerate, sandstones, siltstones, and mudstones. In the western part of the study area, four facies associations are defined: gravelly sheets, sandy sheets, small-scale bars, and fine-grained beds. They are interpreted, from west to east, as a gravel-bed braided fluvial system and a sandy high-sinuosity meandering (HSM) fluvial system (Varela

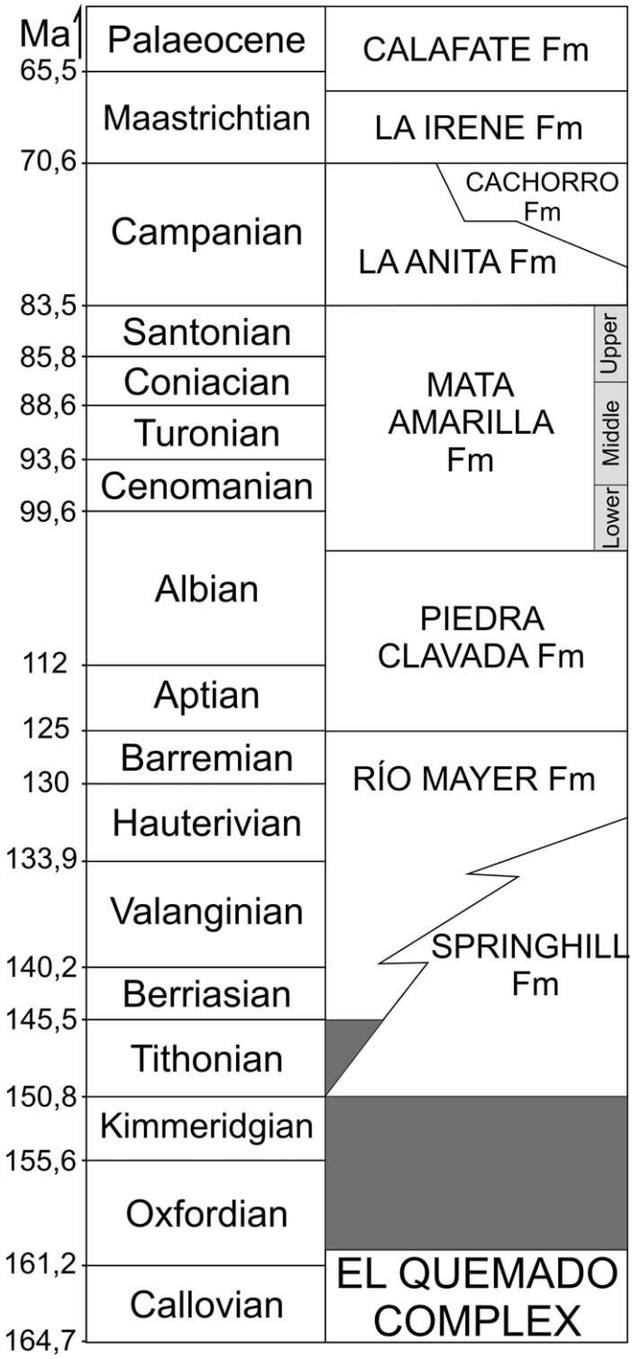

FIG. 2.—General stratigraphic column of the Austral Basin modified from Poiré et al. (2007) and Varela (2011).

2011). In the eastern part of the basin, six facies associations were recognized: complex ribbons, small-scale simple ribbons, small-scale bars, lobes, fine-grained beds, and heterolithic beds with continental fossils. They are part of a low-sinuosity meandering (LSM) fluvial system with aggradation (Varela 2011).

The braided river changes transitionally eastward to a HSM fluvial system with sandy bedload. HSM characterizes localities 9, 11, 12, and 13, while locality 14 shows a transition to a LSM fluvial system with aggradation. This HSM is a tributary of LSM, the main fluvial system within the drainage network. The LSM has a northeast–southwest orientation and flows towards the basin depocenter in the southwest (Varela 2011).

The upper section of the Mata Amarilla Formation is similar to the lower, and consists of fine-grained sediments with paleosols interbedded with shell beds (Varela 2011). In the eastern part of the study area, the littoral facies associations identified i.e., bioclastic lobes, sand bars with herringbone cross-stratification, mudstones with shells pavements, and heterolithic beds with marine fossils are interpreted as littoral marine, lagoon, and estuary paleoenvironments. The western sector of the basin is characterized by two facies associations: large-scale simple ribbons and fine-grained sedimentation, which can be assigned to a distal fluvial system (Varela 2011). The configuration of the basin is similar to the lower section (i.e., a great embayment, Varela 2011).

Facies associations recognized in both the lower and upper sections show conditions of high rate of accommodation/sediment supply, whereas in the middle section rates are low (Varela 2009; Varela 2011). These changes seem to be promoted by relative sea-level oscillations in response to the tectonic evolution of the Patagonian retroarc fold-and-thrust belt (Varela 2009, 2011).

SAMPLING AND METHODS

Sedimentological profiles were described in detail (scale 1:100) in each of the 15 studied localities (Fig. 1). In order to describe the main sedimentary facies, we performed a systematic sampling to carry out the compositional characterization of the Mata Amarilla Formation; abundant paleocurrent data were also obtained to determine the possible source areas.

For the measurement of paleocurrents, both unidirectional and bidirectional, we used a *Brunton*® compass, and the criteria of DeCelles et al. (1983) and Bossi (2007) were followed. Paleocurrents of the lower, middle, and upper sections of the Mata Amarilla Formation were measured in planar cross-bedding, trough cross-bedding, imbricated clasts, and herringbone cross-bedding.

All the paleocurrent data were corrected for magnetic declination according to the date on which they were surveyed. The data were differentiated according to sedimentary units (i.e., fluvial channels, delta front, prodelta channels, estuarine bars). Then, the corrected data were treated statistically with the *Stereonet*® program.

Petrographic and X-ray analyses of each sedimentary facies of the Mata Amarilla Formation as well as samples from the underlying and overlying units (i.e., the top of Piedra Clavada and the base of La Anita formations) were performed.

Conventional petrographic thin sections (30 μm of thickness) were used for textural and compositional analyses. For these a polarization microscope Nikon Eclipse E-200 of the Centro de Investigaciones Geológicas, La Plata, Argentina (CIG) was used. A detailed description of both detrital and diagenetic components was made for each thin section. Detrital components were used to classify the sandstones (according to Folk et al. 1970). Monocrystalline clasts were differentiated considering standard criteria of distinction (extinction, interference color, cleavage, type of twinned, zonation, etc.,), and rock fragments were distinguished in relation to genetic origin (i.e., volcanic (Lv), sedimentary (Ls), metamorphic (Lm), and pyroclastic (Lp)). Furthermore, volcanic clasts were discriminated by their textures as felsitic (Lvf), pilotaxitic (Lvp), and trachytic (Lvt). In minor proportion, lithics are partial to totally altered and were discriminated as indeterminate lithics (Li) (Table A1, see Acknowledgments).

Modal composition was determined on a total of 56 thin sections, 48 from the Mata Amarilla Formation, five from the Piedra Clavada

Formation and three from the La Anita Formation (Table A1). Clasts in each thin section were counted following the Gazzi-Dickinson methodology (Ingersoll et al. 1984), in which 400 points were assessed using a Swift point counter. When rock fragments had monomineral crystals bigger than 0.062 mm, they were considered as crystal clasts (method of Gazzi-Dickinson; Ingersoll et al. 1984).

Characterization of the provenance areas is made more effective when using a combination of several ternary diagrams in order to discriminate different grain properties in the specific end-member combinations (Dickinson and Suczek 1979; Dickinson et al. 1983; Dickinson 1985). Distribution of acidic and intermediate volcanic rock fragments were also represented in a bimodal diagram with the purpose of distinguishing between paleovolcanic and neovolcanic grains (Zuffa 1985, 1987; Critelli and Ingersoll 1995).

A total of 200 fine-grained samples of Piedra Clavada, Mata Amarilla, and La Anita formations from three localities (1, C° Waring, 4, MAFer and 11, the South of Viedma Lake; Fig. 1) were selected for X-ray diffraction (XRD) analysis of whole rock and the clay fraction (< 2 μm). Outcrop sampling was made systematically with spacing of 1 m, and in some cases this was changed according to lithological variations.

Samples for XRD analysis were subjected to soft grinding with a rubber mortar, and repeatedly washed in distilled water until deflocculation occurred. The < 2 μm fraction was separated by gravity settling in suspension, and oriented mounts were prepared on glass slides. Clay mineralogy was determined from diffraction patterns obtained using samples that were air-dried, ethylene glycol-solvated, and heated to 550°C for 2 h (Brown and Brindley 1980). Diffractograms were run on an X PANanlytical model X'Pert PRO diffractometer (CIG), using Cu/Ni radiation and generation settings of 40 kV and 40 mA. Routine air-dried mounts were run between 2 and 32 °2θ at scan speed of 2 °2θ/min. Ethylene glycol-solvated and heated samples were run from 2 to 27 °2θ and 3 to 15 °2θ, respectively, at a scan speed of 2 °2θ/min. Once diffractograms were obtained they were digitally processed with *Origin*® Software, which allows peak identification and conversion of the values from 2θ angles into Å. We then assigned the mineral species to each peak.

From the whole-rock diagram, estimation of mineralogical components is classified according to the following abundances: trace ($< 1\%$); very scarce (1–5%); scarce (5–20%); moderate (20–40%); abundant (40–60%), and very abundant ($> 60\%$) (Tables A2, A3, A4, see Acknowledgments).

Semiquantitative estimations of the relative concentrations of the clay minerals were based on the peak-area method (Biscaye 1965) on glycolated samples (001 for smectite, kaolinite, palygorskite, illite, and mixed layer illite–smectite, and 002 for chlorite, and mixed-layer chlorite–smectite). The response of the mineral species to sedimentation depends on the form of the particles (Pierce and Siegel 1969); for that reason each mineral proportion is not directly proportional to the areas defined. Relative percentages of each clay mineral were determined by applying empirical factors (Moore and Reynolds 1989).

The abundance of different clay minerals in the < 2 μm fraction is summarized in Tables A2, A3, and A4.

More than 30 years of experience in the CIG X-rays laboratory suggests that the 001 area of illite peak (10 Å) corresponds to the entire unit, the 001 peak of kaolinite and 002 of chlorite (~ 7 Å) must be considered as area 2, and the area of the peak of smectite (14 Å) is obtained by area 4. Considering that the peak of maximum intensity of the kaolinite and 002 of the chlorite are located near 7 Å (Lluch and Spalletti 1976), the relative proportions of these mineral species are obtained from the reflections of 002 of kaolinite (3.57 Å) and 004 of chlorite (3.53 Å). The relative quantification of the mixed-layer illite–smectite was calculated from the reflections located between 10 and 14 Å. Smectite crystallinity was determined from the 17 Å (001) peak in the glycolated sample. In this regard, the depth of the valley on the low-angle side of the peak (V) and the height of the peak above the background (P) were obtained following the criteria of Biscaye (1965), which indicate that values of V/P near 1 represent high crystallinity while $V/P < 1$ are indicative of low crystallinity.

PALEOCURRENT ANALYSIS

Paleocurrent data were obtained from the fifteen localities of the study area for each of the three sections of the Mata Amarilla Formation (Fig. 3A–C).

Lower Section

In the western part of the study area, paleocurrent measurements from the distal fluvial paleoenvironment (locality 11) indicate paleoflow towards the SE (Fig. 3A), into an embayment situated in the east. At locality 15 paleocurrents from the delta front, obtained in planar cross-bedding, indicate sediment transport towards the ENE (Fig. 3A). Prodelta channels with imbricated clasts show that paleocurrents flowed towards the ESE (Fig. 3A). Finally, estuarine bars with herringbone cross-bedding display paleocurrents mostly oriented NW–SE, although there is a component to the WSW (Fig. 3A).

In the northeastern part of the study area, at locality 4, paleocurrent measurements in planar cross-bedding from a small delta body indicate a transport direction towards the SSE (Fig. 3A).

Middle Section

Paleocurrent data are divided according to the three main fluvial systems: braided, high-sinuosity meandering (HSM), and low-sinuosity meandering with aggradation (LSM).

At locality 10, in the western part of the study area, the braided fluvial system contains longitudinal bars with imbricated clasts and planar cross-bedding which show paleocurrents with low dispersion towards the SE (Fig. 3B).

In the HSM fluvial system, paleocurrents measured in trough cross-bedding, planar cross-bedding, and imbricated clasts have very high dispersion. At localities 11 and 13 paleocurrents are mostly towards the NNE (Fig. 3B), whereas at localities 12 and 14 they are towards the SSE (Fig. 3B), and finally at locality 9, paleocurrents are towards the NW (Fig. 3B). This high dispersion and disparity in paleocurrent data is typical of a HSM fluvial system.

A LSM fluvial system was observed in outcrops from localities 1, 2, 3, 4, 5, 6, 7, 8, and 15. The paleocurrent measurements obtained mainly from trough cross-bedding, and less frequently in planar cross-bedding, show low dispersion and have a strong paleocurrent vector towards the SSW (Fig. 3B), except for locality 4, where paleocurrents are mainly towards the W (Fig. 3B).

Upper Section

This section is represented at only two localities (14 and 15), and they are characterized as distal fluvial systems. Despite the scarcity of outcrops, it is possible to recognize that channel flow was towards the east (Fig. 3C).

SANDSTONE PETROGRAPHY

The sandstones of Mata Amarilla Formation ($N = 48$; Table A1) are clast supported with scarce protomatrix between 0 and 6%; when pseudomatrix is present it ranges between 7 and 17%. The grain size of detrital components varies between fine- to coarse-grained sand (120–850 μm), and exceptionally some grains are as coarse as 1500 μm. In general, detritus is moderately sorted, and the grains are subrounded to subangular.

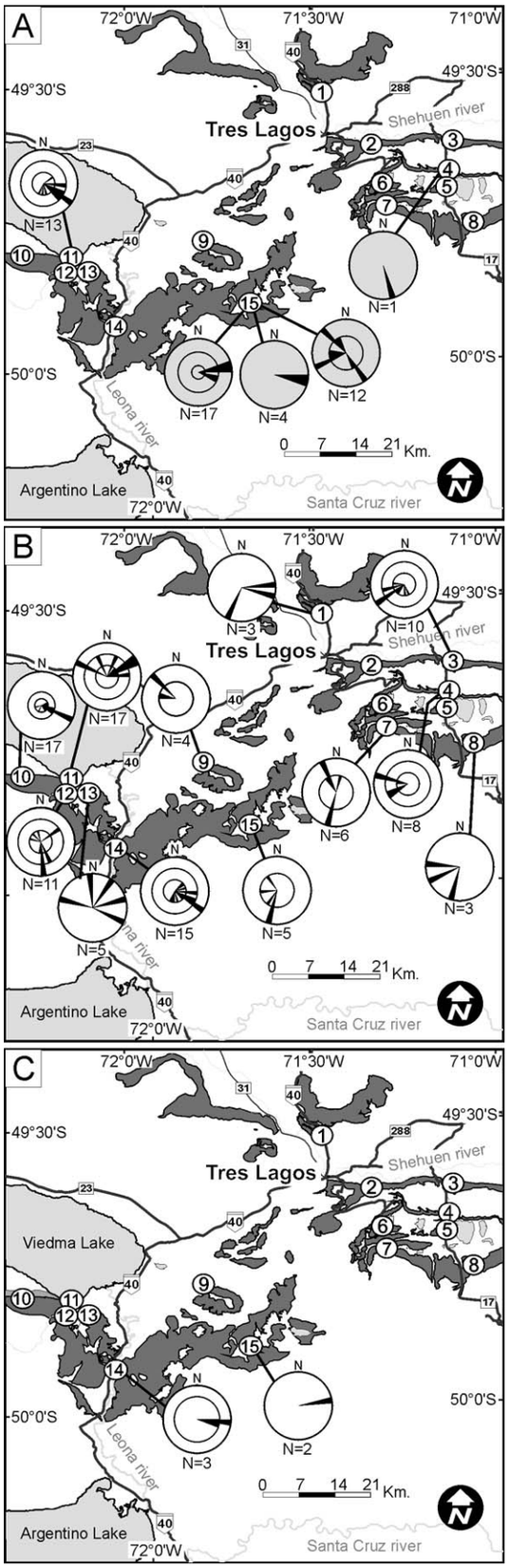

Petrographic analysis allows us to recognize that 70 to 75% of the rock volume is represented by four main components, in order decreasing of abundance: rock fragments, feldspars, monocrystalline quartz, and polycrystalline quartz. Cements are mostly represented by clay, carbonate, and iron oxides. The volume of porosity was determined optically to range from 8% to 30%, and no hydrocarbon impregnation was observed (Table A1).

Detrital Components

Monocrystalline quartz (Qm): this component is present in variable proportions from scarce to abundant (4–42%), with an average of 14%. Crystals (200–600 μm) have straight extinction, commonly with embayments and occasionally with micrographic and runic textures associated with a volcanic origin (Fig. 4A). In some cases, crystal clasts are elongated and show undulating extinction related to a metamorphic origin. The grains are subangular to subrounded, and less commonly, well rounded and fractured.

Polycrystalline quartz (Qp): these grains are scarce to moderate, ranging between 2% and 18%, with an average of 9%. Grains range from coarse sand (~ 1200 μm) to small pebbles. Individual crystals are anhedral, elongate to ribbon-shaped, with undulating extinction and sutured boundaries (Fig. 4B). This points to a metamorphic origin. Sporadically, polycrystalline quartz shows equidimensional crystals with straight boundaries.

Potassium feldspar (Fk): these crystals range from moderate to very abundant (14–44%; ~ 31%), are near 300 μm in size, and are subrounded to subangular, or occasionally well rounded. They show common oscillatory zonation and are twinned according to the Carlsbad law (Fig. 4C), with marked cleavage and, rarely, are fractured. The dominant type is orthoclase in euhedral to subhedral crystals, and in lower proportion, sanidine and microcline are present, displaying typical latticework twinning. Feldspars are frequently altered to sericite and sometimes form pseudomatrix (*sensu* Dickinson 1970).

Plagioclase (Plg): the plagioclase composition varies from oligoclase to andesine. Plagioclases are less abundant than K-feldspars, ranging from 0.5 to 6% (~ 2% on average). The crystals (~ 150 μm) are angular to subangular, and occasionally fractured. They are twinned according to the albite (Fig. 4D) and, less commonly, pericline laws. They rarely show a high degree of alteration to clay minerals and generation of pseudomatrix.

Opaque grains (Op): constituted by subangular to subrounded iron oxide grains, they are present in scarce proportion (< 1.3%) but in some cases rise to 8.3% (Table A1).

Volcanic lithic with felsitic texture (Lvf): the most common volcanic lithic grains (11–42%, ~ 25%), ~ 700 μm in size, are characterized by an internal felsitic texture, which is an aphanitic texture, cryptocrystalline to microcrystalline, formed by an association of small equidimensional and anhedral crystals of quartz and feldspars (Fig. 4E). Felsitic textures are related to volcanic acid groundmass (rhyolites and dacites), though it frequently appears as a recrystallization product of volcanic glass. Volcanic lithics with spherulitic texture are thus also included in this category, interpreted as products of volcanic-glass recrystallization or devitrification. Locally these clasts show variable degrees of alteration to clay minerals, constituting part of the pseudomatrix.

←

FIG. 3.—Geological map of the study area showing paleocurrent rose plots for the three sections of Mata Amarilla Formation. **A)** Lower section: distal fluvial channels (white rose); from left to right gray roses are from: delta front, prodelta channels, estuarine bars, and small delta. **B)** Middle section: paleocurrents of fluvial channels (braided, high sinuosity and low sinuosity with aggradational fluvial systems). **C)** Upper section: paleocurrents of fluvial channels.

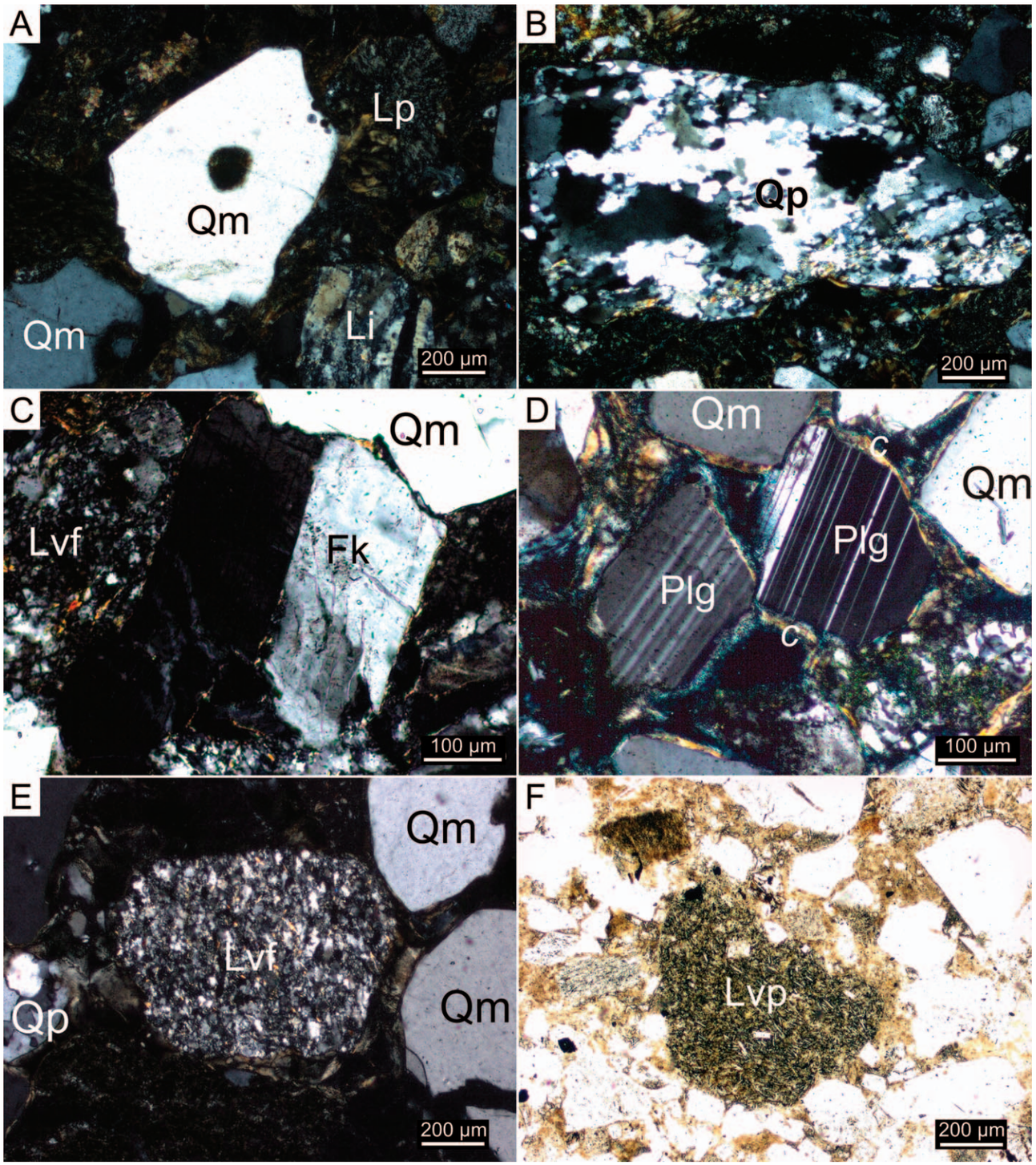

FIG. 4.—Thin-section photomicrographs of representative major framework grains from sandstones of the Mata Amarilla Formation. **A)** Monocrystalline quartz (Qm), indeterminate lithic (Li), and pyroclastic lithic (Lp). **B)** Polycrystalline quartz (Qp). **C)** Potassium feldspar (Fk), volcanic lithic with felsitic texture (Lvf), and monocrystalline quartz (Qm). **D)** Plagioclases (Plg) and monocrystalline quartz (Qm) with clay coatings (*c*). **E)** Volcanic lithic with felsitic texture (Lvf), polycrystalline quartz (Qp), and monocrystalline quartz (Qm). **F)** Volcanic lithic with pilotaxic texture (Lvp).

Volcanic lithic with pilotaxitic texture (Lvp): these are very scarce to scarce (2–8%, ~ 4%), average 600 μm in size, and are frequently altered to clay minerals. Pilotaxitic texture is recognized by the presence of small plagioclase crystals, euhedral to subhedral, immersed in an aphanitic groundmass (Fig. 4F). This texture is characteristic of intermediate volcanic groundmass.

Volcanic lithic with trachytic texture (Lvt): these volcanic lithic grains are the least common (< 1.3%) with an average grain size of ~ 400 μm. Trachytic texture is characterized by small crystals of plagioclase with their major axes oriented parallel, immersed in an aphanitic groundmass. This texture is typical of the intermediate to acid volcanic rocks, especially trachytes, though is also present in andesites and dacites.

Pyroclastic lithic (Lp): these volcanic lithic grains are very scarce to scarce (0–8%), and they are recognized mainly in coarse-grained sandstones (400–800 μm). In these pumice clasts glassy shards can be distinguished, though they are frequently altered to spherulitic or felsitic texture.

Sedimentary lithic (Ls): very scarce to moderate in abundance, these clasts range between 0.3% and 18%, (~ 5%). Most consist of mudstone intraclasts; others are uncommonly fine-grained sandstones. They are rounded, internally structureless, with elongated to subcircular shape and constitute part of the pseudomatrix when altered.

Glauconite lithic (Lg): this particular type of sedimentary lithic is very scarce (0–6%), and they are very well rounded to rounded with clay coatings; they are recognized by the typical greenish color.

Indeterminate lithic (Li): this group includes lithic clasts with intense alteration and cryptocrystalline grains; they represent 2% to 20% of the detrital components and vary in size from 350 to 700 μm. Most come from the alteration of volcanic lithics and feldspars, completely or partially replaced by clay minerals.

Pseudomatrix (PMz): this detrital component is variable between 0% and 17%, and it is the common product of the deformation and alteration of the acid to intermediate volcanic grains and feldspars. It is recognized by postdepositional deformation of labile grains, which are commonly stretched and acquire pore shape.

Cements

Clay cement (Cc): this type of cement is dominant in sandstones of the Mata Amarilla Formation. It consists of clay coatings (Fig. 5A), where primary porosity is preserved. In some cases, clay cements are oriented according to two perpendicular directions by sharp angles forming microslickensides (Fig. 5B). In other cases, they form clay cutans with typical banded microstructure, deposited during successive stages (Fig. 5C). The alternation of different color bands in cutans is due to the presence and absence of reddish iron oxides. Dark bands are related to the presence of organic colloids or manganese oxides. Commonly clay cutans completely occlude the pore space.

Carbonate cement (Ca): calcite is present in some sandstones from the lower and upper sections of the Mata Amarilla Formation, commonly associated with shell beds. It is composed of coarse mosaic calcite that completely closes the pore space (Fig. 5D), though it locally consists of fine mosaic texture. Siderite forms orange nodules, very common in paleosol levels.

Iron oxides cement (Fe-ox): ferruginous cements are observed as big concretions in sandstone levels (Fig. 5E). They are reddish and composed of hematite and magnetite. This cement reduces the primary porosity notably (Fig. 5F), and sometimes nodules and concretions grow in concentric caps.

Sandstone Classification

Sandstones, in decreasing order of abundance, are composed of rock fragments (53%), feldspars (33%), and quartz (14%; Table A1). According to the ternary diagram of Folk et al. (1970), samples are classified as feldspathic litharenites, except DRG 15 and LB 7, which are lithic arkoses (Fig. 6A).

Rock fragments are frequently of volcanic composition with different degrees of alteration, the most common texture being felsitic (Lvf, 25%). Polycrystalline quartz (Qp), mainly of metamorphic origin, constitutes 10% of the total detrital mode, while volcanic lithics with pilotaxitic texture (Lvp, 4%), trachytic texture (Lvt, 0.4%), and pyroclastic lithics (Lp, 0.6%) are subordinate. Sedimentary lithoclasts are variable in abundance in the various samples (Ls, ~ 5%). Glauconite grains (Lg) are present locally in the lower and upper sections of the Mata Amarilla Formation, and are considered products of intrabasinal reworking (i.e., are parautochthonous, *sensu* Amorosi 1995, 1997). Orthoclase is the dominant feldspar (30%), with less abundant (< 1%) sanidine and microcline; plagioclase is less common (2%). Monocrystalline quartz occurs in moderate proportion (14%, Table A1).

SANDSTONE PROVENANCE

Provenance analyses of sandstones obtained from the traditional ternary graphs (QmFLt, QtFL, and QpLvLs of Dickinson et al. 1983 and Dickinson and Suczek 1979) are showed in Figures 6C–E. These methods are accepted and used by many authors (Suczek and Ingersoll 1985; Packer and Ingersoll 1986; Manassero 1988), though they were also discussed by others (Ingersoll 1990; Ingersoll et al. 1993; Critelli and Ingersoll 1995). Detrital modes respond to the interaction of several factors like climate, agent of transport, distance to the source area, and, tectonics and subsidence of the basin; they also depend on diagenetic processes (Dickinson and Suczek 1979; Marsaglia and Ingersoll 1992; Ingersoll et al. 1993; Raingemborn 2006; Gómez-Peral et al. 2011).

Petrofacies

Petrofacies are used to characterize a group of compositionally similar sandstones by the determination of detrital modes, as well as sedimentary provenance (Scasso and Limarino 1997; Limarino et al. 2000; Stefani et al. 2007). Regarding the proportion of monocrystalline quartz (Qm) in the QmFL diagram of Dickinson et al. (1983), two groups of samples can be recognized (Fig. 6B), which are less distinct in QFL (Fig. 6C).

Group A (45 samples): This group is characterized by subordinate monocrystalline quartz less than 35%, and predominance of feldspar and lithics. In this group a distinction can be delineated between samples with more or less than 15% of monocrystalline quartz. Samples with scarce monocrystalline quartz (≤ 15%) plot in the transitional arc and in minor proportion in the undissected arc. The average composition estimated for this subgroup A1 is $Qm_9F_{33}L_{58}$ (Fig. 6B). The other sample set, subgroup A2 (Qm > 15%), is characterized by a mode of $Qm_{23}F_{30}L_{47}$ and corresponds to the transitional-arc field in the ternary provenance diagram (Fig. 6B).

Group B (3 samples): this group is rich in monocrystalline quartz, (Qm > 35%; Fig. 6B). These samples (LB 11, LB 16, and CI 8; Table A1) are characterized by an average mode of $Qm_{40}F_{17}L_{43}$, and in the provenance diagrams plot in the mixed and transitional-recycled fields (Fig. 6B).

The diagram of Dickinson and Suczek (1979) for sandstones with a high proportion of lithics highlights a different sample distribution related to QpLvLs composition (Table A1, Fig. 6D). It is possible to define two petrofacies using this method.

Petrofacies I: This petrofacies is characterized by low proportion of polycrystalline quartz (Qp ≤ 15%) and very high content of volcanic rock fragments (76% in average), of which 85.6% are acid and 14.4% are intermediate. The detrital mode of petrofacies I is $Qp_{10}Lv_{76}Ls_{14}$ (Fig. 6D). Samples of this petrofacies correspond to north-northeast part of the study area (Fig. 1, localities 1–8).

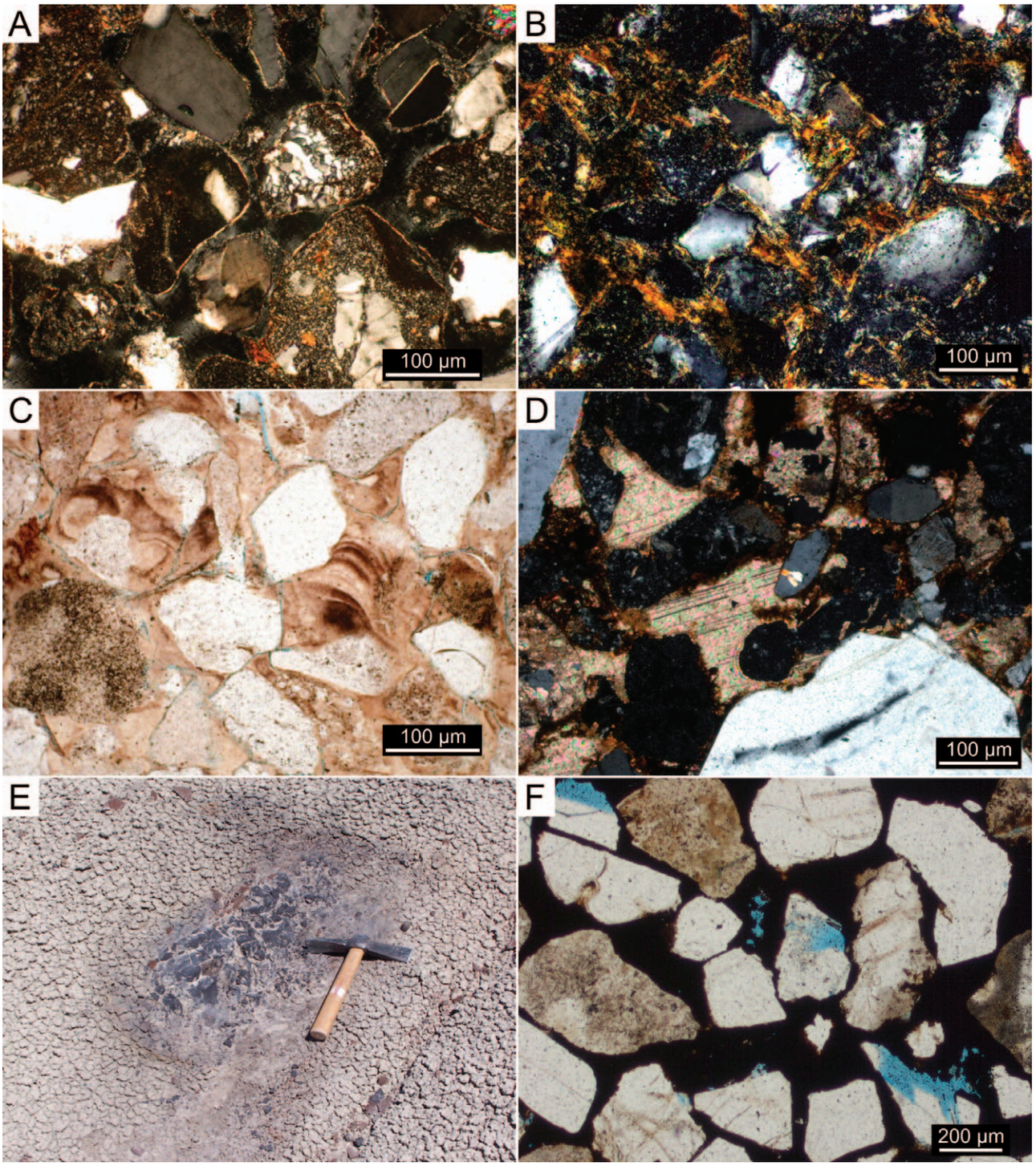

FIG. 5.—Microscopic and macroscopic features of cements. **A)** clay coatings, **B)** clay cement forming microslickensides, **C)** clay cutans, **D)** macrosparite, **E)** pedogenic concretion of iron oxides, **F)** iron oxides cement in thin section.

Petrofacies II: This petrofacies is represented by samples from the western part of the study area (Fig. 1, localities 10–14), characterized by an elevated proportion of polycrystalline quartz (Qp > 15%). The average composition is $Qp_{25}Lv_{63}Ls_{12}$ (Fig. 6D). Volcanic rock fragments (63% on average), constitute 83.1% of acid and 16.9% of intermediate affinity.

Samples from the Piedra Clavada and La Anita formations plot in the transitional-arc field, with La Anita samples closer to the dissected arc

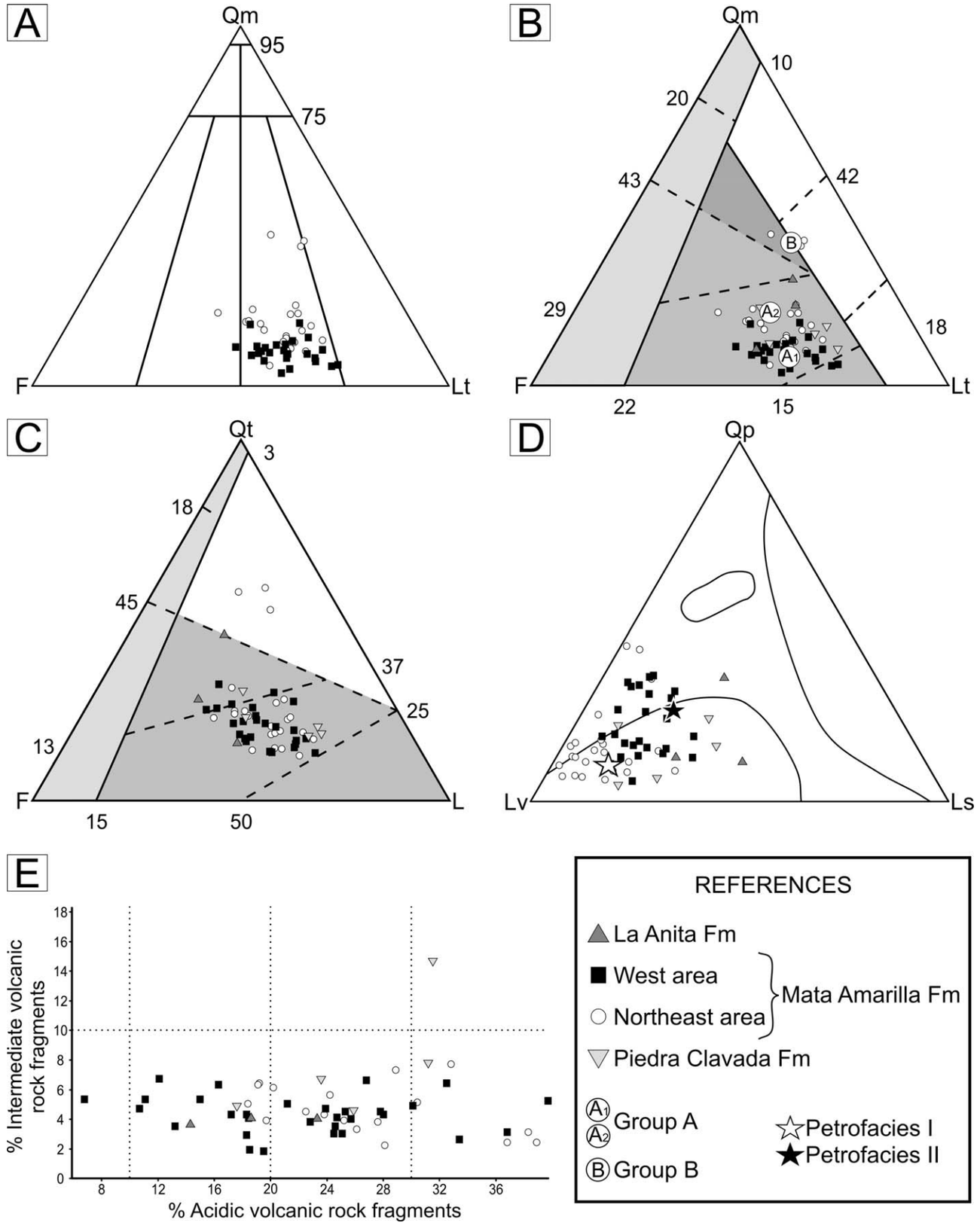
A
Qm
95
75
F
Lt
B
Qm
10
20
43
42
29
18
22
15
F
Lt
B
A2
A1
C
Qt
3
18
45
37
25
13
F
L
15
50
D
Qp
Lv
Ls
E
% Intermediate volcanic rock fragments
% Acidic volcanic rock fragments
REFERENCES
La Anita Fm
West area
Northeast area
Mata Amarilla Fm
Piedra Clavada Fm
A1
A2
Group A
B
Group B
Petrofacies I
Petrofacies II

field (Fig. 6B). However, this sample set is scarce and differs from the composition of the La Anita Formation recorded in the Calafate area (Manassero 1988; Macellari et al. 1989).

According to the QmFLt and QtFL diagrams, no significant compositional differences are distinguished between the three formations (Fig. 6B, C).

The QsLvLs diagram is often used in sandstones with significant lithic grains to differentiate samples derived from orogenic and magmatic-arc environments (Dickinson and Suczek 1979; Hulka and Heubeck 2010). This diagram clearly shows that all the samples analyzed are within the magmatic-arc field (Fig. 6D).

The abundance diagram of acidic versus intermediate volcanic rock fragments does not show a differentiated distribution of the samples (Fig. 6E). However, petrofacies I shows a constrained distribution of the acidic volcanic rock fragments (~ 18–38%); a wider dispersion is observed in petrofacies II (~ 6–40%; Fig. 6E).

X-RAY DIFFRACTION

The results of X-rays diffraction analysis are shown in tables A2, A3, and A4, and make it possible to recognize the compositional signature from three localities of the study area (Fig. 1, localities 1, 4, and 11).

Locality 1.—In this locality, whole-rock compositional data show that quartz is very abundant, alkali feldspar is in moderate to low proportion, and plagioclase is moderate to scarce. Carbonate components are poorly represented by scarce to absent calcite and very scarce to absent dolomite, and siderite appears in very scarce or trace proportion. Hematite, magnetite, and rare pyrite are recognized only in levels with pedogenic nodules and concretions (Fig. 7; 112 meters). Clays range from abundant to scarce, but are commonly in moderate proportion. (Fig. 7, Table A2). Clay-fraction XRD analysis indicates that smectite is the dominant clay mineral (~ 91% on average), being present in all analyzed samples. Kaolinite is associated with siltstone and very fine sandstones (~ 5% on average). Illite and chlorite constitute ~ 1% and ~ 0.5% on average respectively, though both clay minerals have higher proportions in beds with iron nodules and concretions (Fig. 7, Table A2). The presence of moderately abundant palygorskite is recognized mainly in the lower section of the Mata Amarilla Formation. At locality 1, the dominant clay minerals of the Piedra Clavada Formation are kaolinite (34% on average) and smectite (17%), with a minor proportion of illite (~ 8%), chlorite (~ 8%), and mixed-layer clays present as illite–smectite (~ 8%) and chlorite–smectite (~ 7%). The clay fraction of the La Anita Formation is composed mainly of kaolinite (~ 68%), with smectite (~ 17%), chlorite (~ 3%), illite (~ 2%), and illite–smectite (~ 9%) and chlorite–smectite (~ 3%, Table A2, Fig. 7) as mixed-layer clays.

Locality 4.—Whole-rock compositional data show quartz as the predominant component, and plagioclase in moderate to low proportion, with alkali feldspars very scarce. Carbonate minerals are associated with shell beds in the lower section of the Mata Amarilla Formation; they occur as calcite, dolomite, and, less frequently, siderite (Fig. 8, Table A3). Clay minerals appear in moderate proportion and are dominated by smectite (~ 95%) with small quantities of illite (~ 2%), kaolinite (~ 1%), and traces of illite–smectite mixed-layer clay (Table A3, Fig. 8).

Locality 11.—Whole-rock XRD analysis indicates that quartz is very abundant, with plagioclase and potassium feldspar in smaller proportion. Calcite is scarce in the lower section, and is very scarce to absent in the rest of the unit. Dolomite and siderite display the same trend (Fig. 9). Gypsum is represented only in the lower section of the Mata Amarilla Formation (Fig. 9, level of 17 meters). Clay minerals are scarce in whole-rock samples; the ≤ 2 μm fraction shows that smectite is dominant (88% on average, Table A4, Fig. 9). In contrast, illite is scarce (6% on average), and decreases progressively from the lower section to the upper part of the unit. Kaolinite averages 6%, and mixed-layer illite–smectite are only scarcely represented in the lower section and the basal-middle section of the Mata Amarilla Formation (Fig. 9, Table A4).

Clay-Mineral Assemblages

Four clay-mineral assemblages can be identified in Mata Amarilla Formation on the basis of the presence, type, and relative abundance of the clay minerals. The clay-mineral assemblages are termed S (rich in smectite), S-K (rich in smectite and kaolinite), Pg (rich in palygorskite) and I/S (rich in mixed-layer illite–smectite with subordinate smectite content).

S Assemblage.—The most common clay association in the Mata Amarilla Formation, it is represented in the three studied localities by more than 90% of samples analyzed (Tables A2, A3, A4). The S assemblage is characterized by very abundant smectite, and varies between 75 and 100%. In minor proportions, kaolinite (1–20%), mixed-layer I/S (0–11%), and illite (0–6%) are present (Fig. 10A).

S-K Assemblage.—Recognized only in the middle and upper sections of the Mata Amarilla Formation in locality 1 (Table A2), the assemblage consists of smectite (34–67%), and kaolinite (32–64%) (Fig. 10B). This association is restricted to levees and crevasse deposits (Varela 2011).

Pg Assemblage.—This association is restricted to the lower section of the Mata Amarilla Formation (Fig. 7, Table A2, A3, A4), and is interpreted as lagoon, estuary, and coastal-plain environments (Varela et al. 2011). The palygorskite is recognized in the ≤ 2 μm diffractograms by its main peak located between 10.29 and 10.32Å (Moore and Reynolds 1989). This represents less than 5% of the sample set and is composed of abundant palygorskite (25–67%) and smectite (25–70%), with scarce kaolinite (0–10%) and rare chlorite (0–3%) (Fig. 10C, Table A2).

I/S assemblage.—Recognized in the Mata Amarilla Formation (Table A4), this clay-mineral assemblage is commonly associated with the top of paleosol profiles developed over continental or littoral marine deposits (Varela et al. 2011). The presence of abundant mixed-layer I/S (56–85%), less common smectite (7–27%), and subordinate illite (0–10%) associated with scarce kaolinite (3–9%) defines this assemblage (Fig. 10D). Mixed-layer illite–smectite (I/S) is characterized by a high proportion of expansive layers (ranging between 50% and 80%), which is related to a random I/S ratio (R = 0; Pollastro 1993) and the 001 reflection is near 11.4 Å.

Smectite clays in S, S-K, and Pg assemblages have sharp peaks and well-defined reflections (with V/P of 0.9 in average), indicating high crystallinity. However, the S-I assemblage shows smectite with moderate to low crystallinity (with V/P of 0.5 on average). Considering smectite composition suggested by some authors (Grim and Güven 1978; Dananaj et al.

←

FIG. 6.—Detrital modes of the Mata Amarilla Formation sandstones. **A)** sandstone classification (Folk et al. 1970); **B**, **C)** traditional provenance diagrams (Dickinson et al. 1983); **D)** provenance diagram for sandstones with a high proportion of lithic (modified from Dickinson and Suczek 1979); **E)** intermediate versus acidic volcanic rock fragments.

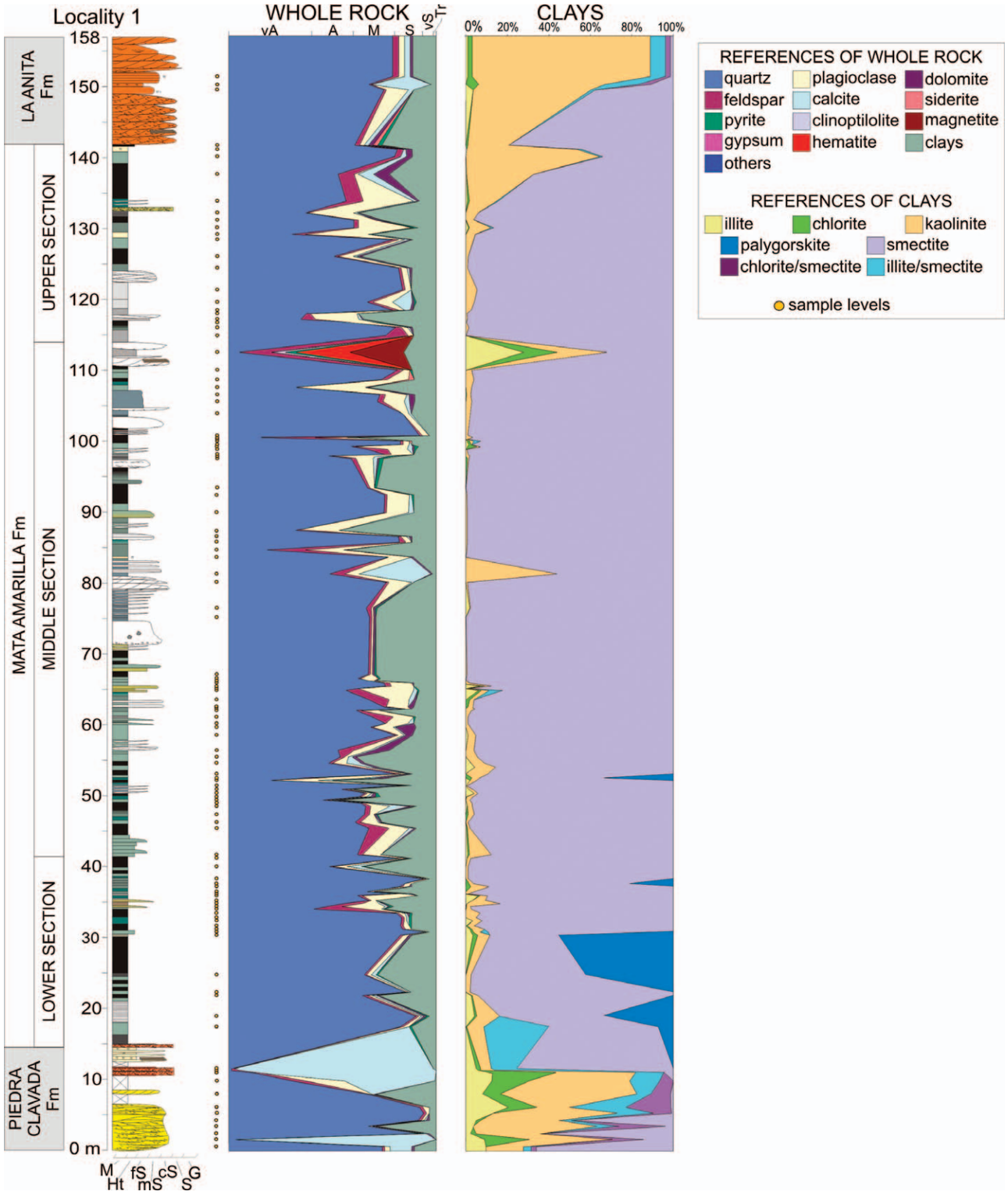

FIG. 7.—Sedimentological section of the Mata Amarilla Formation at C° Waring (locality 1), showing vertical distribution of sedimentary facies and X-ray diffraction composition sheet from whole rock and clay fraction.

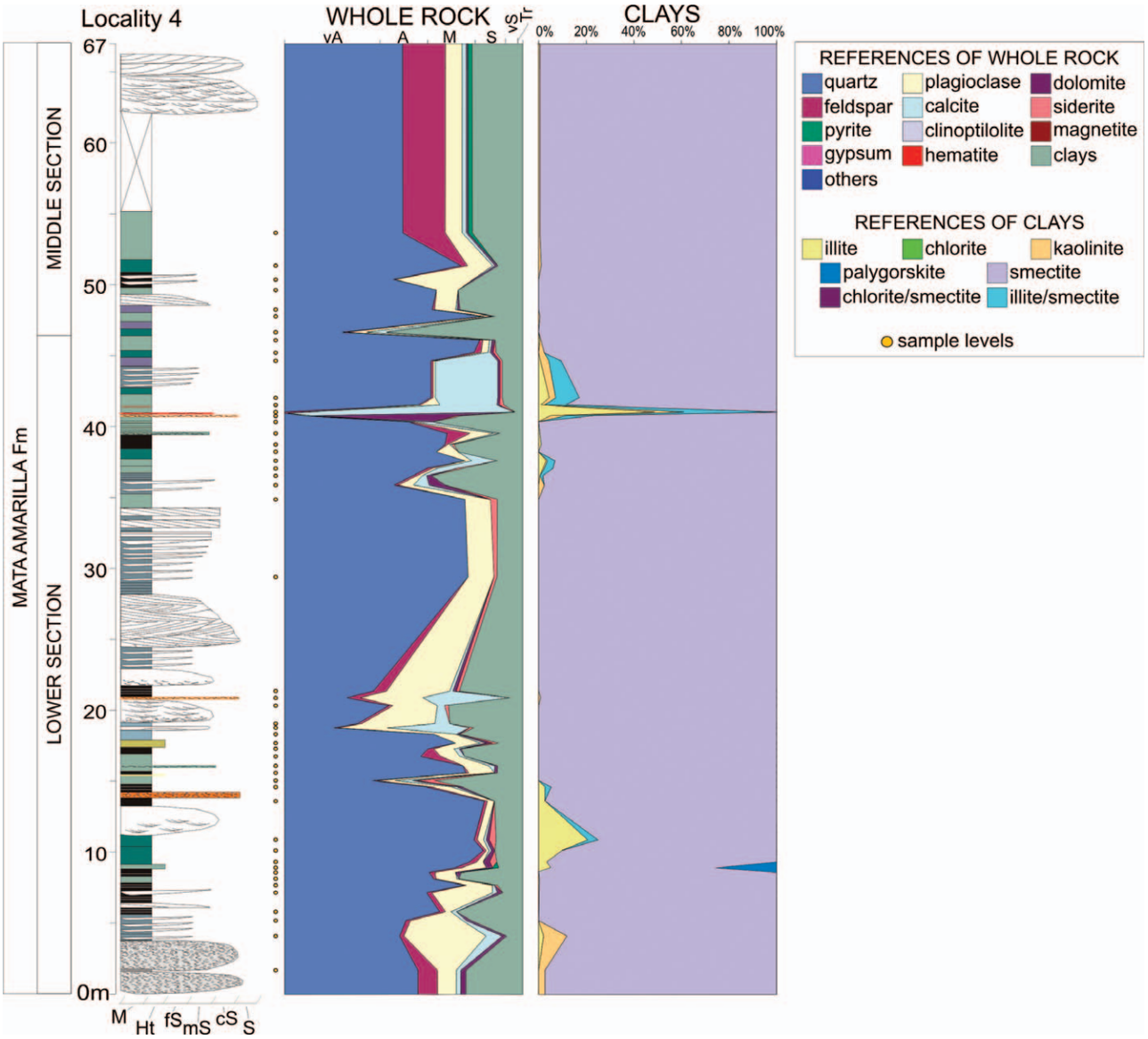

FIG. 8.—Sedimentological section of the Mata Amarilla Formation at locality 4, showing vertical distribution of sedimentary facies and X-ray diffraction composition sheet from whole rock and clay fraction.

2005), X-ray spectra show that 001 reflections of smectite vary between 12.3 to 12.8 Å on air-dried samples (Fig. 10), suggesting Na or Mg interlayer occupancy rather than Ca. An exception is at locality 4, where the lower section shows calcium smectite (001 reflections ~ 14.4 to 15.1 Å).

PEDOGENESIS–EODIAGENESIS

Postdepositional processes recognized in the Mata Amarilla Formation are dominated by clay cementation, evidenced by thin coatings (Fig. 5A) and by clay cutans, in which consecutive stages of eluviation and illuviation can be observed (Fig. 5C). Clay coatings promote the preservation of primary porosity of the rock because quartz and feldspar overgrowths are inhibited in their presence. Cutans are also common in the paleosols identified and are considered to be controlled by typical illuviation processes (Fig. 5C; Varela et al. 2006; Varela 2010; Varela et al. 2012b).

The presence of magnetite and hematite cements in the upper section of the Mata Amarilla Formation (Fig. 7) is directly related to pedogenic iron nodules, common in poorly drained paleosols.

Carbonate cementation is less frequent and is associated mostly with the lower and upper sections of the Mata Amarilla Formation (Table A1). It is usually composed of coarse mosaic calcite, commonly as blocky cement (Fig. 5D). Ferruginous and magnesium carbonate cements are very scarce, and form small nodules or spherical concretions of siderite (Fig. 5F) or blocky dolomitic cement, respectively. This typical cementation is considered to be controlled by the deposition of shell beds and marine-meteoric diagenesis in subsurface and oxygenated conditions.

Sandstone porosity of the Mata Amarilla Formation is mainly primary, although some secondary porosity was observed as the result of partial or total dissolution of lithic fragments, and less frequently, associated with the fracturing of lithic and feldspar clasts. Petrographic analyses estimate

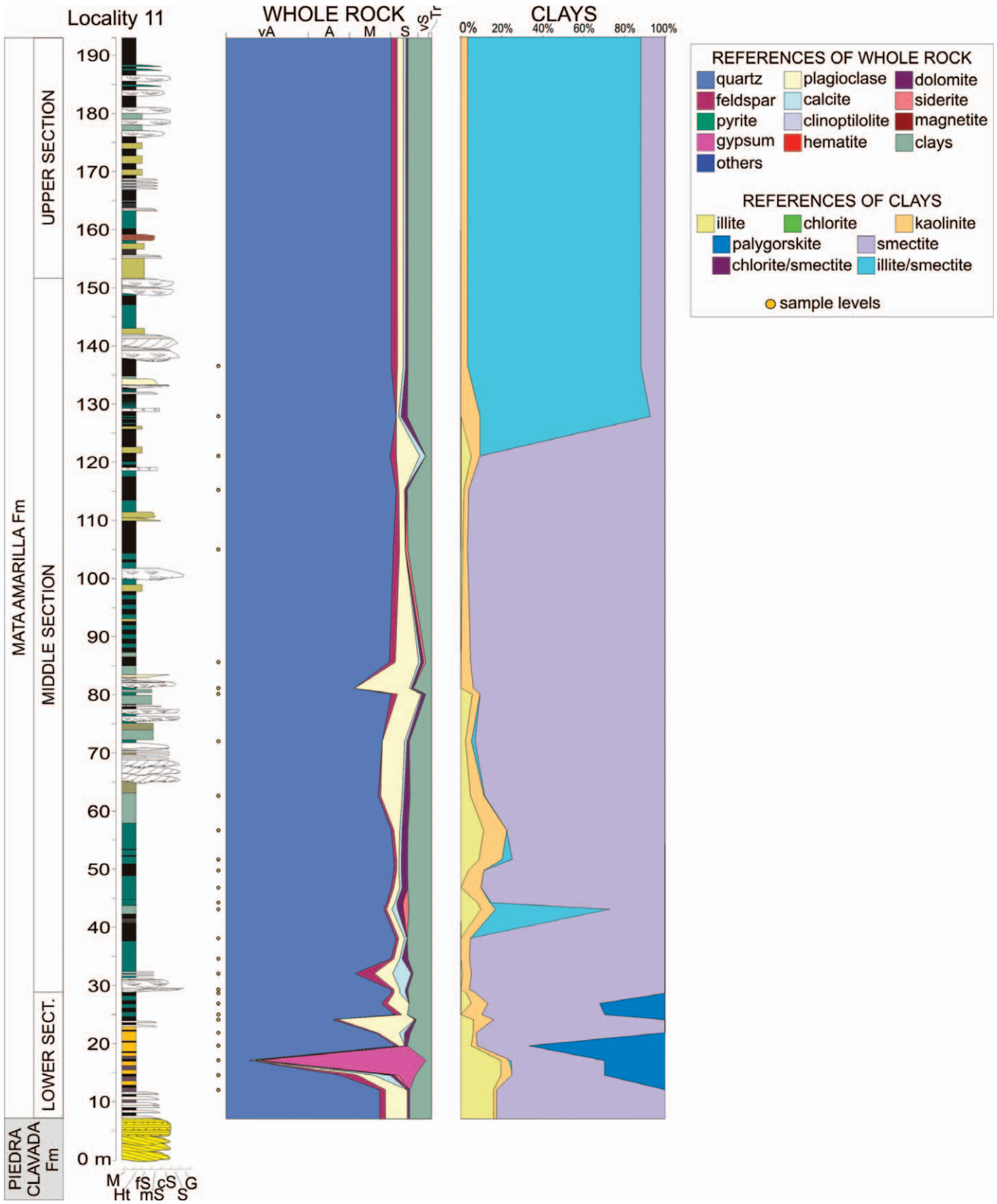

FIG. 9.—Sedimentological section of the Mata Amarilla Formation at south of Viedma Lake (locality 11), showing vertical distribution of sedimentary facies and X-ray diffraction composition sheet from whole rock and clay fraction.

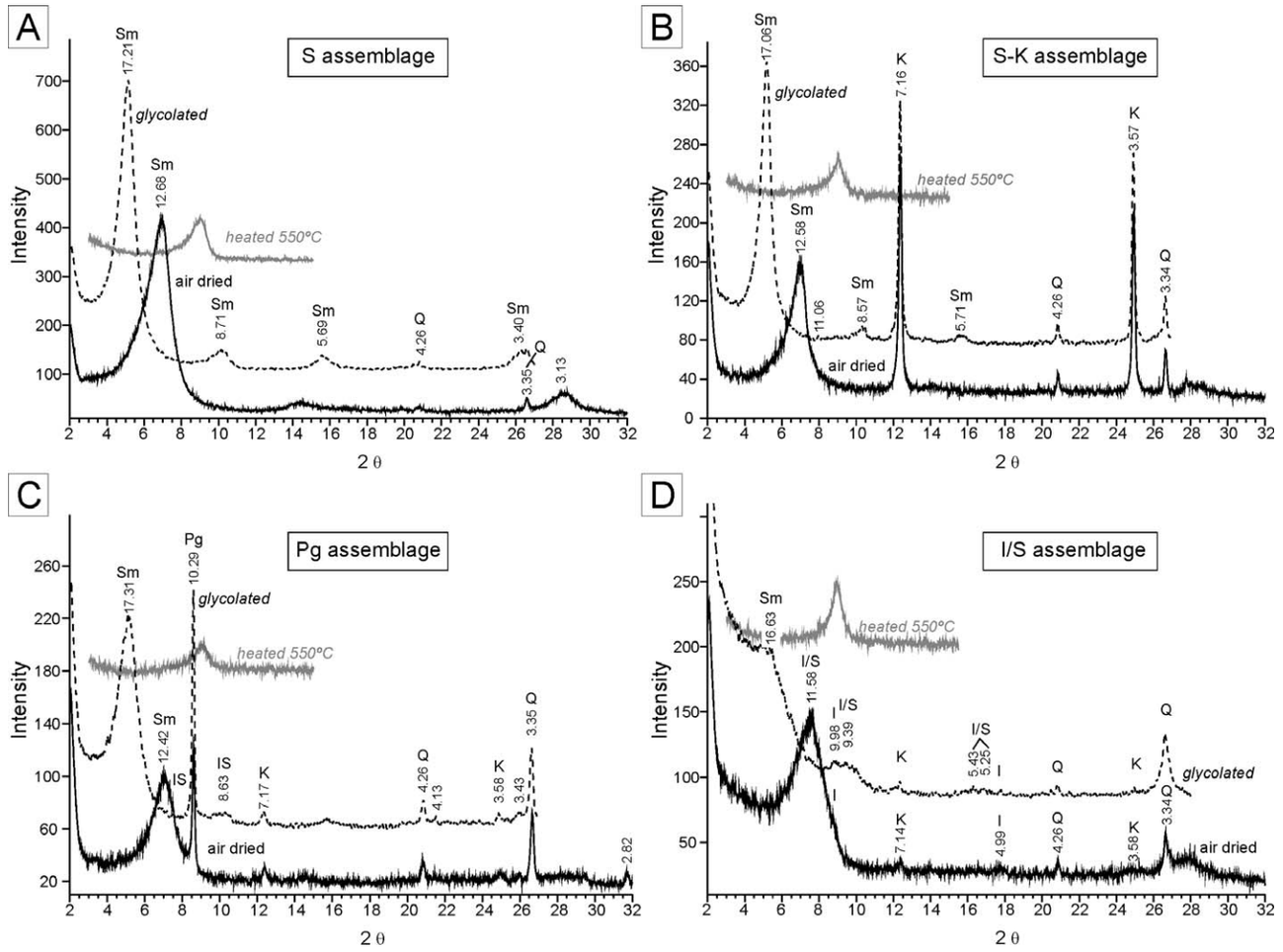

FIG. 10.—Diffractograms of clay-mineral assemblages of Mata Amarilla Formation. **A)** S assemblage, **B)** S-K assemblage, **C)** Pg assemblage, **D)** I/S assemblage.

that porosity is high to very high (ranging between 5 and 25%), with an average of 16%. In the middle section of study unit porosity reaches approximately 30% (Table A1).

Clay-mineral analyses indicate that smectite is the dominant clay mineral in the complete sedimentary succession, and is related to the weathering products of volcanic glass mass with K^+ as the dominant interlayer cation (Masuda et al. 1996). The crystallinity of this clay mineral decreases with the progress of weathering.

Also observable is the neoformation of kaolinite and I/S, related to pedogenesis during the eodiagenetic regime and controlled by paleoenvironmental conditions.

DISCUSSION

Sandstone Provenance

According to the QmFLt diagram (Fig. 6B), two different group of samples are distinguished, taking into account Qm proportions. Group A ($Qm \leq 35\%$) shows a transitional-arc provenance while group B ($Qm > 35\%$) shows mixed to transitional recycled-orogen provenance. Despite the low dispersion of the samples of group A, it was possible to identify two subgroups; A1 (less than 15% of Qm) are samples from the west of the study area, whereas A2 (Qm between 15 and 35%) shows provenance from the northeast of the study area. Group B is represented by samples from localities 9 and 15 in the central part of the study area (Fig. 11), and are characterized by higher proportions of Qt associated with a major time and transport distance regarding its relative position in the Austral Foreland Basin (Fig. 11).

Further interpretations can be drawn from the QpLvLs diagram (Dickinson and Suczek 1979), in which two petrofacies are easily discriminated. Samples of petrofacies I are found in the northeast of the study area and the source area is located farther to the northeast according to the paleocurrent dataset (Figs. 3, 5E, 11). Determined by paleocurrent data, the source area of petrofacies II is located to the west-southwest, and samples are found at localities in the west of the study area (Figs. 3, 5E, 11). The discrimination of these two petrofacies is based on the fact that petrofacies I shows higher Lv and lower Qp than petrofacies II. This can be explained by the difference in composition of the source areas. The source area for petrofacies I corresponds to rocks formed by Jurassic bimodal volcanism (Deseado Massif, Fig. 11), and petrofacies II is sourced by the uplifted orogen (Late Cretaceous Patagonian fold-and-thrust belt), composed of metamorphic and volcanic complexes (Fig. 11), which drive an increase in Qp of metamorphic origin.

The bimodal diagram of acidic versus intermediate volcanic rock fragments shows a restricted distribution of acidic volcanic rock fragments in petrofacies I and a wide dispersion in petrofacies II (Fig. 6E). This differentiation can be attributed to a lesser contribution of

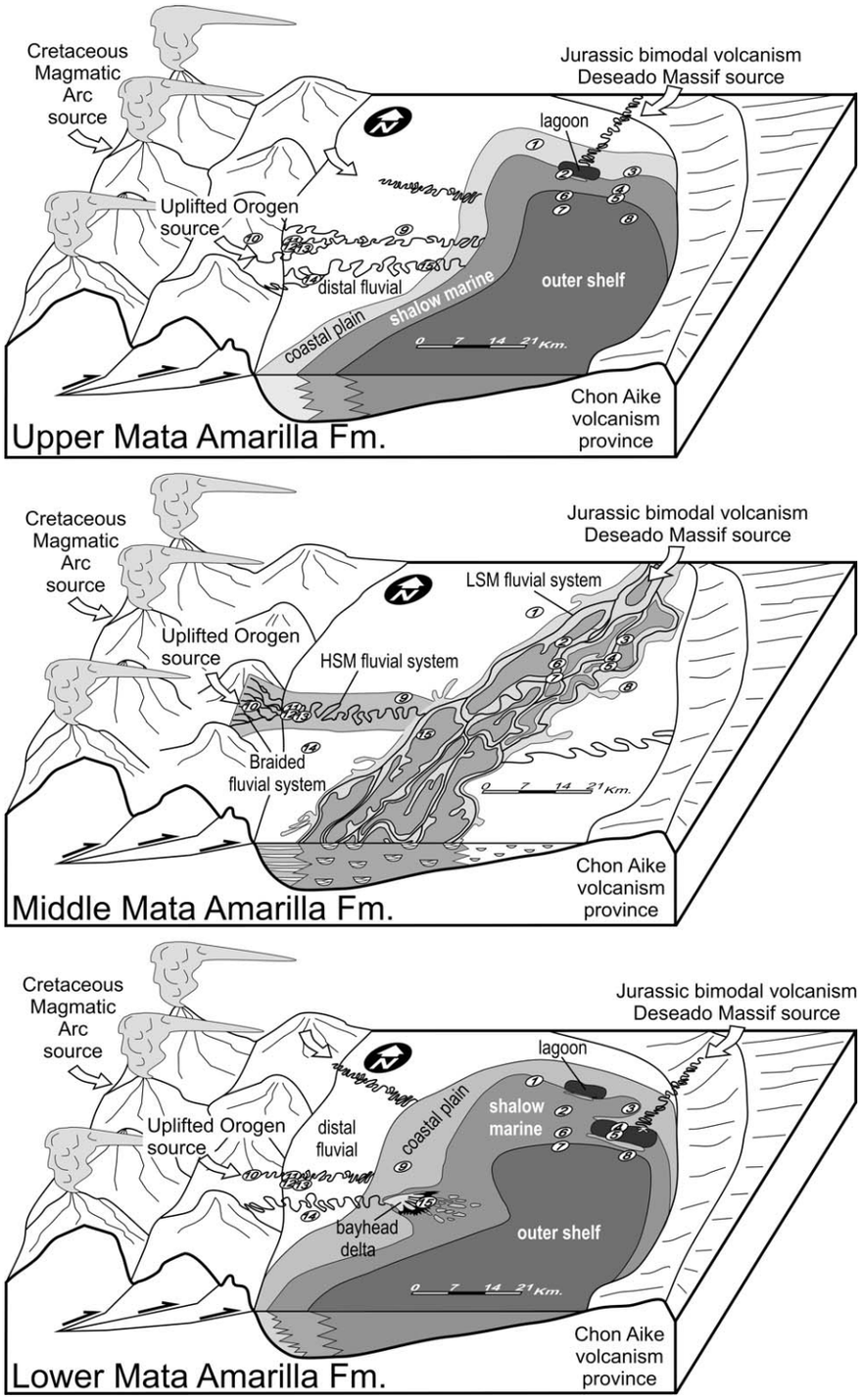

FIG. 11.—Block diagrams showing proposed source areas of the Austral Foreland Basin during the Late Cretaceous and their relationship with the paleoenvironmental and paleogeographic context (Mata Amarilla Formation). No vertical scale.

acidic volcanic rock fragments from the west compared to in northeastern provenance areas. However, no distinctive discrimination can be observed from the intermediate volcanic rock fragments (Fig. 6E). With respect to volcanic detritus, the high mean proportion of felsitic volcanic grains in both petrofacies can be compared with other analogues such as synrift sediments in the Mariana region (Marsaglia and Devaney 1995), Lau Basin (Clift 1995) and Sumisu rift (Taylor et al. 1990), and the felsic petrofacies of the Gran Cañon Formation (Critelli et al. 2002).

Both acidic and intermediate volcanic rock fragments are altered by intense weathering and pedogenesis under favorable climatic conditions (Cenomanian greenhouse period). According to the criteria of Zuffa (1985, 1987) and Critelli and Ingersoll (1995), a different degree of

alteration of volcanic rock fragments from Jurassic and a contemporary Cretaceous arc is not observed.

For that reason, the volcanic lithoclasts (Lv) of petrofacies II may have been contributed from a Cretaceous contemporary magmatic arc or from extensive Jurassic bimodal volcanism (El Quemado Complex, Ibañez and Tobífera formations). It is important to remark that both the synrift rocks of the El Quemado complex and the Deseado Massif rocks share the same lithology (Pankhurst et al. 2000). However, during the evolution of the Foreland Austral Basin, the El Quemado Complex was part of the uplifted orogen while the Deseado Massif was located in an intracontinental position (Fig. 11). Under these two different geotectonic settings, detrital modes and volcanic rock fragments are not significantly different, demonstrating the importance of paleocurrent data to the integrated study.

Pankhurst et al. (1998) proposed that the geochemical signature of the Jurassic Deseado Massif volcanism differs from that of the Austral Basin rift volcanism (El Quemado Complex, Ibáñez and Tobífera formations). Further investigations in the form of more detailed geochemical analyses of the provenance of the Mata Amarilla Formation could discriminate these two different volcanic events.

Environmental Controls on Clay-Mineral Associations

The dominance of smectite, formed by alteration of volcanic glass coming from contemporaneous Late Cretaceous ash fall, is likely the result of intense pedogenesis under a greenhouse climatic context. Illitization of smectite is commonly related to burial-depth transformation; however, other authors have suggested this process to be associated with superficial environments commonly seen in vertisols (Mora et al. 1998) as a pedogenic product (Gonçalves et al. 2006). In this study we recognize the presence of authigenic mixed-layer illite–smectite near the superficial horizons of paleosols. In this regard, it is widely suggested that substitution and incorporation of K^+ in interlayer sites of smectite promotes illite formation (Hower et al. 1976; Masuda et al. 1996). Moreover, organic acids, evolved during an eodiagenetic regime, have been shown to be critical in the formation of illite from smectite (Small 1993).

Smectite typically decreases in crystallinity towards the top of the paleosol profiles, in direct relation to pedogenic processes. The low grade of crystallinity observed is in relation to the transformation of smectite to mixed-layer illite–smectite.

For instance, kaolinitization of smectite can be associated with periods of interaction with phreatic fluids of low pH in levees and crevasse deposits of the Mata Amarilla Formation. This is related to high topographic relief with well-drained to moderately drained conditions, which drives a wash of high-solubility ions (Na^+ and K^+), promoting the generation of kaolinite over smectite (Retallack 2001; Varela 2011). In opposition, low topographic relief favors the preservation of sodium and potassium ions concentrated in smectite (Retallack 2001).

The presence of palygorskite is associated with paleosols formed under inefficient drainage conditions (Velde 1985; Pozo and Martin de Vidales Rodriguez 1989; Mayayo et al. 2008; Huerta and Armenteros 2009). Huerta and Armenteros (2009) also mention the presence of palygorskite associated with dolomite and interpret its origin as a product of precipitation in ephemeral saline lakes in the presence of sulfates, favored by bacterial reduction processes. In this sense, the palygorskite identified in the lower section of the Mata Amarilla Formation is related to coastal environments where paleosols developed under poorly drained conditions. The origin of dolomite could be linked to simultaneous chemical precipitation in the same conditions. The precipitation of both dolomite and palygorskite in natural environments has been linked to microbial activity in coastal lagoons and salt lakes today (Vasconcelos et al. 1995; Vasconcelos and Mackenzie 1997; Huerta and Armenteros 2009).

Finally, vertical variations in clay-mineral proportions in the studied sections reveal a strong environmental control on distribution (Figs. 7, 8, 9). In this sense, the increase of illite and kaolinite from smectite is related to paleosol development in different hydrodynamic and topographic-relief conditions (Varela et al. 2012b). The kaolinitization of smectite is favored by intense lixiviation under well drained conditions and high topographic relief, whereas under poorly drained conditions and low topographic relief, illitization occurs (Gonçalves et al. 2006; Varela et al. 2012b).

CONCLUSIONS

- Sandstones of the Mata Amarilla Formation are classified as feldspathic litharenites, except two samples which are lithic arkoses.
- Glauconite grains are considered as parautochtonous in origin because of the restriction of their occurrence to shallow marine deposits of the lower and upper transgressive sections of the Mata Amarilla Formation.
- The main provenance of the sandstones of the Mata Amarilla Formation was a magmatic arc, and to a much lesser extent, an orogenic area composed of uplifted volcanic and metamorphic rocks. Moreover, underlying and overlying units also reflect tentatively a magmatic-arc provenance.
- The relative proportion of acidic versus intermediate volcanic rock fragments of both petrofacies is not an accurate criterion to discriminate similar volcanic source areas with different ages and geographic positions.
- The degree of alteration of the volcanic rock fragments is directly linked to pedogenesis and weathering under greenhouse climatic conditions, and not as a result of differing age of the volcanic sources.
- X-ray diffraction analyses indicate the presence of four clay-mineral assemblages identified in three sections of the Mata Amarilla Fm: S (rich in smectite), S-K (rich in smectite and kaolinite), Pg (rich in palygorskite), and I/S (rich in mixed-layer illite–smectite with subordinate smectite content).
- The source area of petrofacies I (northeastern part of the study area) corresponds to Jurassic bimodal volcanic rocks of the Deseado Massif. The source area of petrofacies II (western part of the study area) corresponds to the uplifted orogen (Patagonian fold-and-thrust belt) composed of metamorphic and volcanic complexes.
- The preponderance of smectite is related to the alteration of volcanic glass mass associated with ash fall from contemporaneous Cretaceous arc volcanism.
- Increased illite and kaolinite from smectite transformation is related to paleosol development in different conditions of hydrodynamic and topographic relief.
- Palygorskite and dolomite in the lower section of the Mata Amarilla Formation formed as a result of early diagenesis or pedogenesis in coastal environments with poorly drained paleosols.
- Finally, this study demonstrates that the combination of paleocurrent data, petrography, and clay mineralogy provide a better understanding of this foreland basin, which could be used as an analogy to other foreland basins along the Andes.

ACKNOWLEDGMENTS

We would like to thank to J. Maggi, C. Genazzini, and P. Garcia for their help in XRD analysis, to D. Mártire and M. Pausada for the preparation of thin sections, to A. Iglesias, A. Zamuner, J. Cuitiño, and G. Pedersen for the assistance in the field, and to G.M. Casal for English review. The authors are very grateful to reviewers T. Lawton, S. Critelli, and M. Manassero, and to AE L. De Ros for highly constructive reviews. Thank to T.J. Maguire and U. Zimmermann for refining the sentence structure and grammar. This research

was financially supported by the Consejo Nacional de Investigaciones Científicas y Técnicas (PIP 1016 to D.G. Poiré). Four tables are available from JSR's Data Archive: http://sepm.org/pages.aspx?pageid=229.

REFERENCES

Adatte, T., Keller, G., and Stinnesbeck, W., 2002, Late Cretaceous to early Paleocene climate and sea-level fluctuations: the Tunisian record: Palaeogeography, Palaeoclimatology, Palaeoecology, v. 178, p. 165–196.

Ameghino, F., 1906, Les formations sédimentaires du Crétacé Superieur et du Tertiaire de Patagonia, avee an paralèlle entre leurs faunes mammalogiques et celles de l' ancient continent: Museo Nacional de Buenos Aires, Anales, v. 15, p. 1–568.

Amorosi, A., 1995, Glaucony and sequence stratigraphy: a conceptual framework of distribution in siliciclastic sequences: Journal of Sedimentary Research, v. 65, p. 419–425.

Amorosi, A., 1997, Detecting compositional, spatial, and temporal attributes of glaucony: a tool for provenance research: Sedimentary Geology, v. 109, p. 135–153.

Arbe, H.A., 1989, Estratigrafía, discontinuidades y evolución sedimentaria del Cretácico en la Cuenca Austral, Prov. de Santa Cruz, *in* Chebli, G., and Spalletti, L.A., eds., Cuencas Sedimentarias Argentinas: Instituto Superior de Correlación Geológica, Universidad Nacional de Tucumán, Serie de Correlación Geológica, v. 6, p. 419–442.

Arbe, H.A., 2002, Análisis estratigráfico del Cretácico de la Cuenca Austral, *in* Haller, M.J., ed., Geología y Recursos Naturales de Santa Cruz: XV Congreso Geológico Argentino, p. 103–128.

Biddle, K., Uliana M., Mitchum R., Jr., Fitzgerald, M., and Wright R., 1986, The stratigraphic and structural evolution of central and eastern Magallanes Basin, Southern America, *in* Allen, P., and Homewood, P., eds., Foreland Basins: International Association of Sedimentologists, Special Publication 8, p. 41–61.

Biscaye, P.E., 1965, Mineralogy and sedimentation of recent deep sea clay in the Atlantic Ocean and adjacent seas and oceans: Geological Society of America, Bulletin, v. 76, p. 803–832.

Bossi, G.E., 2007, Análisis de Paleocorrientes: San Miguel de Tucumán, Ediciones Magna, 200 p.

Brown G, and Brindley G.W., 1980, X-ray diffraction procedures for clay mineral identification, *in* Brindley, G.W., and Brown, G., eds., Crystal Structures of Clay Minerals and their X-Ray Identification: London, Mineralogical Society, p. 305–359.

Cavazza, W., and Ingersoll, R.V., 2005, Detrital modes of the Ionian Forearc Basin fill (Oligocene–Quaternary) reflect the tectonic evolution of the Calabria–Peloritani Terrane (Southern Italy): Journal of Sedimentary Research, v. 75, p. 268–279.

Chamley, H., 1989, Clay Sedimentology: Berlin Springer-Verlag, 623 p.

Clift, P.D., 1995, Volcaniclastic sedimentation and volcanism during the rifting of western Pacific backarc basins, *in* Taylor, B., and Natland, J., eds., Active Margins and Marginal Basins of the Western Pacific: American Geophysical Union, Monograph 88, p. 67–96.

Critelli, S., and Ingersoll, R.V., 1995, Interpretation of neovolcanic versus paleovolcanic sand grains: an example from Miocene deep marine sandstones of the Topanga Group (Southern California): Sedimentology, v. 42, p. 783–804.

Critelli, S., Marsaglia, K.M., and Busby, C.J., 2002, Tectonic history of Jurassic backarc-basin sequence (the Gran Cañon Formation, Cedros Island, Mexico), based on compositional modes of tuffaceous deposits: Geological Society of America, Bulletin, v. 114, p. 515–527.

Dananaj, I., Frankovska, J., and Janotka, I., 2005, The influence of smectite content on microstructure and geotechnical properties of calcium and sodium bentonites: Applied Clay Science, v. 28, p. 223–232.

Decelles, P.G., Langford, R.P., and Schwartz, R.K., 1983, Two new methods of paleocurrent determination from trough cross-stratification: Journal of Sedimentary Petrology, v. 53, p. 629–642.

Dickinson, W.R., 1970, Interpreting detrital modes of graywacke and arkose: Journal of Sedimentary Petrology, v. 40, p. 695–707.

Dickinson, W.R., and Rich, E.I., 1972, Petrologic intervals and petrofacies in the Great Valley Sequence, Sacramento Valley, California: Geological Society of America, Bulletin, v. 83, p. 3007–3024.

Dickinson, W.R., 1985, Interpreting provenance relations from detrital modes of sandstones, *in* Zuffa, G.G., ed., Provenance of Arenites: Dordrecht, D. Reidel Publishing Co., p. 333–361.

Dickinson, W.R., and Suczek, C., 1979, Plate tectonics and sandstone composition: American Association of Petroleum Geologists, Bulletin, v. 63, p. 2164–2182.

Dickinson, W.R., Beard, L.S., Brakenridge, G.R., Erjavec, J.L., Ferguson, R.C., Inman, K.F., Knepp, R.A., Lindberg, F.A., and Ryberg, P.T., 1983, Provenance of North American Phanerozoic sandstones in relation to tectonic setting: Geological Society of America, Bulletin, v. 94, p. 222–235.

Do Campo, M., del Papa, C., Nieto, F., Hongn, F., and Petrinovic, I., 2010, Integrated analysis for constraining palaeoclimatic and volcanic influences on clay-mineral assemblages in orogenic basins (Palaeogene Andean foreland, Northwestern Argentina): Sedimentary Geology, v. 228, p. 98–112.

Fildani, A., and Hessler, A.M., 2005, Stratigraphic record across a retroarc basin inversion: Rocas Verdes–Magallanes Basin, Patagonian Andes, Chile: Geological Society of America, Bulletin, v. 117, p. 1596–1614.

Fildani, A., Cope, T.D., Graham, S.A., and Wooden, J.L., 2003, Initiation of the Magallanes Foreland basin: timing of the southernmost Patagonian Andes orogeny revised by detrital zircon provenance analysis: Geology, v. 31, p. 1081–1084.

Folk, R.L., Andrews, P.B., and Lewis, D.W., 1970, Detrital sedimentary rock classification and nomenclature for use in New Zealand: New Zealand Journal of Geology and Geophysics, v. 13, p. 937–968.

Fosdick, J.C., Romans, B.W., Fildani, A., Bernhardt, A., Calderón, M., and Graham, S.A., 2011, Kinematic evolution of the Patagonian retroarc fold-and-thrust belt and Magallanes foreland basin, Chile and Argentina, 51°30′S: Geological Society of America, Bulletin, v. 123, p. 679–1698.

Fossa Mancini, E., Feruglio, E., and Yussen de Campana, J.C., 1938, Una Reunión de geólogos de Y.P.F. y el problema de la Terminología Estratigráfica: Boletín de Informaciones Petroleras, Buenos Aires, v. 171, p. 31–95.

Gómez-Peral, L.E., Raigemborn, M.S., and Poiré, D.G., 2011, Petrología y evolución diagenética de las facies silicoclásticas del Grupo Sierras Bayas, Sistema de Tandilia, Argentina: Latin American Journal of Sedimentology and Basin Analysis, v. 18, p. 3–41.

Gonçalves, D.F., Rossetti, D., Truckenbrodt, W., and Mendes, A.C., 2006, Argilominerais da Formaçao Codó Grajaú, Nordeste do Brasil: Latin American Journal of Sedimentology and Basin Analysis, v. 13, p. 59–75.

Grim, R.E. and Güven, N., 1978, Bentonites; Geology, Properties and Uses: Amsterdam Elsevier, Developments in Sedimentology 24, 256 p.

Hower, J., Eslinger, E.V., Hower, M.E., and Perry, E.A., 1976, Mechanism of burial metamorphism of argillaceous sediments, Mineralogical and chemical evidence: Geological Society of America, Bulletin, v. 87, p. 725–737.

Huerta, P., and Armenteros, I., 2009, Formación de Dolomita Asociada a Procesos de Sulfato Reducción Bacteriana en Lagos Salinos Efímeros del Paleógeno de la Cuenca de Almazán: Sociedad Española de Mineralogía, Revista, v. 11, p. 105–106.

Hulka, C., and Heubeck, C., 2010, Composition and provenance history of Late Cenozoic sediments in Southeastern Bolivia: implications for Chaco Foreland Basin evolution and Andean uplift: Journal of Sedimentary Research, v. 80, p. 288–299.

Ingersoll, R.V., 1983, Petrofacies and provenance of late Mesozoic Forearc Basin, Northern and Central California: American Association of Petroleum Geologists, Bulletin, v. 67, p. 1125–1142.

Ingersoll, R.V., 1990, Actualistic sandstone petrofacies: discriminating modern and ancient source rocks: Geology, v. 18, p. 733–736.

Ingersoll, R.V., Bullard, T.F., Ford, R.L., Grimm, J.P., Pickle, J.D., and Sares, S., 1984, The effect of grain size on detrital modes: A test of the Gazzi–Dickinson point-counting method: Journal of Sedimentary Petrology, v. 54, p. 103–116.

Ingersoll, R.V., Kretchmer, A.G., and Valles, P.K., 1993, The effect of sampling scale on actualistic sandstone petrofacies: Sedimentology, v. 40, p. 937–953.

Inglès, M., and Anadón, P., 1991, Relationship of clay minerals to depositional environment in the non-marine Eocene Pontils Group, SE Ebro Basin (Spain): Journal of Sedimentary Petrology, v. 61, p. 926–939.

Inglès, M., and Ramos-Guerrero, E., 1995, Sedimentological control on the clay mineral distribution in the marine and non-marine Palaeogene deposits of Mallorca (Western Mediterranean): Sedimentary Geology, v. 94, p. 229–243.

Iñiguez Rodríguez, A.M., and Decastelli, O.O., 1984, Mineralogía y Diagénesis de arcillas en las formaciones Cretácico–Teciarias de la Cuenca Austral: 9th Congreso Geológico Arcentino, Actas III, p. 402–414.

Leanza, A.F., 1972, Andes Patagónicos Australes, *in* Leanza A.F., ed., Geología Regional Argentina: Academia Nacional de Ciencia de Córdoba, p. 689–706.

Limarino, C., Net, L., Gutiérrez, P., Barreda, V., Caselli, A., and Ballent, S., 2000, Definición litoestratigráfica de la Formación Ciénaga del Río Huaco (Cretácico Superior), Precordillera central, San Juan, Argentina: Asociación Geológica Argentina, Revista, v. 55, p. 83–99.

Lluch, J.J., and Spalletti, L.A., 1976, Minerales de las arcillas en los sedimentos actuales de la región del Cerro San Lorenzo, provincia de Santa Cruz: Asociación Geológica Argentina, Revista, v. 31, p. 23–32.

Macellari, C.E., Barrio, C.A., and Manassero, M.J., 1989, Upper Cretaceous to Paleocene depositional sequences and sandstone petrography of southwestern Patagonia (Argentina and Chile): Journal of South American Earth Sciences, v. 2, p. 233–239.

Manassero, M.J., 1988, Petrología y procedencia de las areniscas cretácicas superiores de la Cuenca Austral Argentina: Asociación Geológica Argentina, Revista, v. 43, p. 175–187.

Marsaglia, K., and Devaney, K.A., 1995, Tectonic and magmatic controls on backarc basin sedimentation: The Mariana region reexamined, *in* Taylor, B., ed., Back-Arc Basins: Tectonics and Magmatism: New York, Plenum Press, p. 497–520.

Marsaglia, K., and Ingersoll, R., 1992, Compositional trends in arc-related, deep marine sand and sandstone: a reassessment of magmatic provenance: Geological Society of America, Bulletin, v. 104, p. 1637–1649.

Masuda, H., O'neil, J.R., Jiang, W.T., and Peacor, D.R., 1996, Relation between interlayer composition of authigenic smectite, minerals assemblages, I/S reaction rate and fluid composition in silic ash of the Nanakai Trough: Clays and Clay Minerals, v. 44, p. 443–459.

Mayayo, M.J., Yuste, A., Luzón, A., and Bauluz, B., 2008, Filosilicatos en un sistema lacustre carbonatado Oligo-Mioceno (Cuenca del Ebro). Implicaciones paleoambientales: Sociedad Española de Mineralogía, Revista v. 9, p. 153–154.

Moore, D.M., and Reynolds, R.C., Jr., 1989, X-Ray Diffraction and the Identification and Analysis of Clay Minerals: Oxford, U.K., Oxford University Press, 329 p.

Mora, C.A., Sheldon, B.T., Elliot, W.C., and Driese, S.G., 1998, An oxygen isotope study of illite and calcite in three Appalachian Paleozoic vertic paleosols: Journal of Sedimentary Research, v. 68, p. 456–464.

Net, L., 2002, Factores de control sobre los tipos de cementos en areniscas carboníferas de la Cuenca Paganzo, noroeste de Argentina: Asociación Argentina de Sedimentología, Revista, v. 9, p. 1–30.

Net, L., Alonso, S., and Limarino, C., 2002, Source rock and environmental control on clay mineral associations, Lower section of Paganzo Group (Carboniferous), Northwest Argentina: Sedimentary Geology, v. 152, p. 183–199.

O'Gorman, J.P., and Varela, A.N., 2010, The oldest lower Upper Cretaceous plesiosaurs (Reptilia, Sauropterygia) from the southern Patagonia, Argentina: Ameghiniana, v. 47, p. 447–459.

Packer, B.M., and Ingersoll, R.V., 1986, Provenance and petrology of Deep Sea Drilling Project sands and sandstones from the Japan and Mariana forearc and backarc basins: Sedimentary Geology, v. 51, p. 5–28.

Pankhurst, R.J., Leat, P.T., Sruoga, P., Rapela, C.W., Márquez, M., Storey, B.C., and Riley, T.R., 1998, The Chon Aike province of Patagonia and related rocks in West Antarctica: a silicic large igneous province: Journal of Volcanology and Geothermal Research, v. 81, p. 113–136.

Pankhurst, R.J., Riley, T.R., Fanning, C.M., and Kelley, S.P., 2000, Episodic silicic volcanism in Patagonia and Antarctic Peninsula: chronology of magmatism associated with the break-up of Gondwana: Journal of Petrology, v. 41, p. 605–625.

Pierce, J.W., and Siegel, F.R., 1969, Quantification in clay mineral studies of sediments and sedimentary rocks: Journal of Sedimentary Petrology, v. 39, p. 187–193.

Poiré, D.G., Zamuner, A.B., Goin, F., Iglesias, A., Canessa, N., Larriestra, C.N., Varela, A.N., Calvo Marcillese, L., and Larriestra, F., 2004, Ambientes sedimentarios relacionados a las tafofloras de las formaciones Piedra Clavada y Mata Amarilla (Cretácico), Tres Lagos, Cuenca Austral, Argentina: 10th Reunión Argentina de Sedimentología, San Luís, p. 140–141.

Poiré, D.G., Franzese, J.R., Spalletti, L.A., and Matheos, S.D., 2007, Estratigrafía de las rocas reservorios de la Cuenca Austral en el sector cordillerano, provincia de Santa Cruz, Argentina, Unpublished field trip guide: Centro de Investigaciones Geológicas, La Plata, 112 p.

Pollastro, R.M., 1993, Considerations and applications of the illite/smectite geothermometer in hydrocarbon-bearing rocks of Miocene to Mississippian age: Clays and Clay Minerals, v. 41, p. 119–133.

Pozo Rodríguez, M., and Martín de Vidales, J.L., 1989, Condiciones de formación de paligorskita–sepiolita en litofacies dolomíticas de la cubeta de Piedrabuena. Campo de Calatrava (Ciudad Real): Estudios Geológicos, v. 45, p. 177–193.

Raingemborn, M., 2006, Análisis composicional y procedencia de la Formación Peñas Coloradas, Grupo Río Chico (Paleoceno superior–Eoceno?), en la región oriental de la Cuenca del Golfo de San Jorge, Chubut, Argentina: Latin American Journal of Sedimentology and Basin Analysis, v. 13, p. 65–87.

Retallack, G.J., 2001, Soils of the Past: An Introduction to Paleopedology, Second Edition: Oxford, U.K., Blackwell Science, 404 p.

Richiano, S., 2012, Sedimentología e icnología de la Formación Río Mayer, Cuenca Austral, Provincia de Santa Cruz, Argentina [Ph.D. Thesis]: Universidad Nacional de La Plata, Facultad de Ciencias Naturales y Museo, 278 p.

Rodríguez, J.F., and Miller, M., 2005, Cuenca Austral, *in* Chebli, G., et al., eds., Frontera Exploratoria de la Argentina: Mar del Plata, 6th Congreso de Exploración y Desarrollo de Hidrocarburos, p. 308–323.

Russo, A., and Flores, M.A., 1972, Patagonia Austral Extraandina, *in* Leanza, A.F., ed., Geología Regional Argentina: Academia Nacional de Ciencias de Córdoba, p. 707–725.

Russo, A., Flores, M.A., and Di Benedetto, H., 1980, Patagonia Austral Extraandina, *in* Turner, J.C.M., ed., Segundo Simposio de Geología Regional Argentina: Academia Nacional de Ciencias de Córdoba, II, p. 1431–1462.

Scasso, R.A., and Limarino, C.O., 1997, Petrología y Diagénesis de Rocas Clásticas: Asociación Argentina de Sedimentología, Publicación Especial 1, 259 p.

Small, J.S., 1993, Experimental determination of the rates of precipitation of authigenic illite and kaolinite in the presence of ácueos oxalate and comparison to the K/Ar ages of authigenic illite in reservoir sandstones: Clay and Clay minerals, v. 41, p. 191–208.

Spalletti, L.A., and Franzese, J.R., 2007, Mesozoic Paleogeography and Paleoenvironmental evolution of Patagonia (Southern South America), *in* Gasparini, Z., Salgado, L., and Coria, R.A., eds., Patagonian Mesozoic Reptiles: Indiana University Press, Bloomington, p. 29–49.

Spalletti, L.A., Queralt, I., Matheos, S.D., Colombo, F., and Maggi, J., 2008, Sedimentary petrology and geochemistry of siliciclastic rocks from the upper Jurassic Tordillo Formation (Neuquén Basin, western Argentina): implications for provenance and tectonic setting: Journal of South American Earth Sciences, v. 25, p. 440–463.

Stefani, C., Fellin, M.G., Zattin, M., Zuffa, G., Dalmonte, C., Mancin, N., and Zanferrari, A., 2007, Provenance and paleogeographic evolution in a multi-source foreland: the Cenozoic Venetian–Friulian Basin (NE Italy): Journal of Sedimentary Research, v. 77, p. 867–887.

Suczek, C.A., and Ingersoll, R.A., 1985, Petrology and provenance of Cenozoic sand from the Indus cone and Arabian basin, DSDP sites 221, 222, and 224: Journal of Sedimentary Petrology, v. 55, p. 340–346.

Taylor, B., Brown, G., Fryer, P., Gill, J.B., Hochstaedter, A.G., Hotta, H., Langmuir, C.H., Leinen, M., Nishimura, A., and Urabe, T., 1990, Alvin–Seabeam studies of the Sumisu Rift, Izu–Bonin arc: Earth and Planetary Science Letters, v. 100, p. 127–137.

Umazano, A.M., Bellosi, E., Visconti, G., and Melchor, R.N., 2008, Mechanisms of aggradation in fluvial systems influenced by explosive volcanism: an example from the Late Cretaceous Bajo Barreal Formation, San Jorge Basin, Argentina: Sedimentary Geology, v. 203, p. 213–228.

Umazano, A.M., Bellosi, E., Visconti, G., Jalfin, G., and Melchor, R.N., 2009, Sedimentary record of a Late Cretaceous volcanic arc in central Patagonia: petrography, geochemistry and provenance of fluvial volcaniclastic deposits of the Bajo Barreal Formation, San Jorge Basin, Argentina: Cretaceous Research, v. 30, p. 749–766.

Varela, A.N., 2009, Accommodation/sediment supply fluvial deposition controlled by base level changes and relative sea level fluctuations in the Mata Amarilla Formation (Early Upper Cretaceous), Southern Patagonia, Argentina: 9th International Conference on Fluvial Sedimentology, Actas Geológica Lilloana, v. 21, p. 66.

Varela, A.N., 2010, Palaeosol development in response to extrinsic and intrinsic factors: The Mata Amarilla Formation (lower Upper Cretaceous), an example of southern Patagonia [abstract], *in* Schwarz, E., Georgieff, S., Piovano, E., and Ariztegui, D., eds., Abstracts Volume: 18th International Sedimentological Congress, Mendoza, Argentina, p. 892.

Varela, A.N., 2011, Sedimentología y Modelos Deposicionales de la Formación Mata Amarilla, Cretácico de la Cuenca Austral, Argentina [Ph.D. Thesis]: Universidad Nacional de La Plata, Facultad de Ciencias Naturales y Museo, 287 p.

Varela, A.N., and Poiré, D.G., 2008, Paleogeografía de la Formación Mata Amarilla, Cuenca Austral, Patagonia, Argentina [abstract]: 12th Reunión Argentina de Sedimentología, Buenos Aires, Actas, p. 183.

Varela, A.N., Poiré, D.G., Richiano S, and Zamuner A, 2006, Los paleosuelos asociados al bosque petrificado María Elena, Formación Mata Amarilla, Cuenca Austral, Patagonia, Argentina [abstract]: 4 Congreso Latinoamericano de Sedimentología y 11 Reunión Argentina de Sedimentología, Bariloche, p. 235.

Varela, A.N., Richiano S, and Poiré, D.G., 2008, Análisis paleoambiental de la Formación Mata Amarilla a partir de su malacofauna, Cuenca Austral, Patagonia, Argentina, *in* Schiuma, M., ed., Trabajos Técnicos: 7th Congreso de Exploración y Desarrollo de Hidrocarburos, p. 601–605.

Varela, A.N., Richiano S, and Poiré, D.G., 2011, Tsunami vs storm origin for shell bed deposits in a lagoon environment: an example from the Upper Cretaceous of Southern Patagonia, Argentina: Latin American Journal of Sedimentology and Basin Analysis, v. 18, p. 63–85.

Varela, A.N., Poiré, D.G., Martin, T., Gerdes, A., Goin, F.J., Gelfo, J.N., and Hoffmann, S., 2012a, U-Pb zircon constraints on the age of the Cretaceous Mata Amarilla Formation, Southern Patagonia, Argentina: its relationship with the evolution of the Austral Basin: Andean Geology, v. 39, p. 359–379.

Varela, A.N., Veiga, G.D., and Poiré, D.G., 2012b, Sequence stratigraphic analysis of Cenomanian greenhouse palaeosols: a case study from southern Patagonia, Argentina: Sedimentary Geology, v. 271–272, p. 67–82.

Vasconcelos, C., and McKenzie, J., 1997, Microbial mediation of modern dolomite precipitation and diagenesis under anoxic conditions (Lagoa Vermelha, Rio de Janeiro, Brazil): Journal of Sedimentary Research, v. 67, p. 378–390.

Vasconcelos, C., McKenzie, J., Bernasconi, S., Grujic, D., and Tien, A.J., 1995, Microbial mediation as a possible mechanism for natural dolomite formation at low temperatures: Nature, v. 377, p. 220–222.

Velde, B., 1985, Clay Minerals: A Physicochemical Explanation of Their Occurrence: Amsterdam, Elsevier, Developments in Sedimentology 40, 427 p.

Wilson, T.J., 1991, Transition from back-arc to foreland basin development in southernmost Andes: Stratigraphic record from the Ultima Esperanza District, Chile: Geological Society of America, Bulletin, v. 103, p. 98–111.

Zattin, M., Stefani, C., and Martin, S., 2003, Detrital fission-track analysis and petrography as keys of Alpine exhumation: the example of the Veneto foreland (Southern Alps, Italy): Journal of Sedimentary Research, v. 73, p. 1051–1061.

Zuffa, G.G., 1985, Optical analysis of arenites: influence of methodology on compositional results, *in* Zuffa, G.G., ed., Provenance of Arenites: NATO-ASI Series C: Mathematical and Physical Sciences: Dordrecht, D. Reidel, p. 165–189.

Zuffa, G.G., 1987, Unravelling hinterland and offshore palaeogeography from deep-water arenites, *in* Leggett, J.K., and Zuffa, G.G., eds., Marine Clastic Sedimentology–Concepts and Case Studies (a volume in memory of C. Tarquin Teale): London, Graham and Trotman, p. 39–61.

Received 6 June 2012; accepted 24 November 2012.